ISSN: 0975-8585

Research Journal of Pharmaceutical, Biological and Chemical Sciences

Quantum-Chemical Study of the Cytotoxic Activity of Pyrimidine–Benzimidazol Hybrids against MCF-7, MGC-803, EC-9706 and SMMC-7721 Human Cancer Cell Lines.

Juan S. Gómez-Jeria* and Andrés Robles-Navarro.

Quantum Pharmacology Unit, Department of Chemistry, Faculty of Sciences, University of Chile. Las Palmeras 3425, Santiago 7800003, Chile.

ABSTRACT

We present a study of the relationships between the electronic structure and the cytotoxicity against four human cancer cell lines of a group of pyrimidine–benzimidazol hybrids. The electronic structure of all the molecules was calculated within the Density Functional Theory at the B3LYP/6-31g(d,p) level with full geometry optimization. For all cell lines, we found statistically significant relationships between the variation of the cytotoxicity and the variation of the values of several local atomic reactivity indices belonging to a common molecular skeleton. An enlarged common skeleton produced better results. The corresponding partial pharmacophores associated with high inhibitory activity were proposed for both common skeletons of each cell line. The merging of the two partial pharmacophores should help the experimentalists in the search of new compounds. The nature of the results obtained here strongly suggests that the molecules act at a single site in each cell line.

Keywords: QSAR, quantum chemistry, DFT, reactivity indices, cytotoxicity, MCF-7, MGC-803, EC-9706, SMMC-7721.

***Corresponding author**

ISSN: 0975-8585

INTRODUCTION

Cytotoxicity (CT) is defined as the quality of being toxic to cells. A toxic molecule may lead to cell necrosis, to a decrease in cell viability or to apoptosis. The main goal of the experimental measurement of toxicity in large series of molecules is the discovery of compounds that are selective against tumor cells while keeping healthy cells unharmed. This is attested by the great number of papers published during this year (2015) [1-24]. Cytotoxic effects can be checked by evaluating the cell membrane integrity (propidium iodide assay, lactate dehydrogenase assay). A different technique is employing the 3-(4,5-dimethyl-2-thiazolyl)-2,5-diphenyl-2H-tetrazolium bromide (MTT) assay.

Viable cells with active metabolism change MTT into a purple colored formazan product. A dead cell loses the ability to convert MTT into formazan, so color formation serves as an appropriate marker of only the viable cells. The quantity of formazan (supposed to be directly proportional to the quantity of viable cells) is measured by recording changes in absorbance at 570 nm. There are several other methods. On the other hand, one of the roles of quantum chemistry is to carry out studies on the relationship between the electronic structure of these molecules and their cytotoxic activity.

They should lead to the building of pharmacophores (a theoretical construct showing the microscopic characteristics of the action site), the detection of atoms involved in the activity and the suggestion of atoms serving as sites of substitution for improved cytotoxicity and/or selectivity. A searching of the literature shows that numerous series of molecules have been tested for CT against a given cancer cell line (MCF-7 for example). We have not found a paper integrating the results obtained from these very different series into a unique interaction model. This is probably due to the lack of formal structure-cytotoxicity relationships studies (SCR).

The only way to integrate the results into a unified interaction model is by carrying out the theoretical studies with exactly the same methodology (*ab initio* Hartree-Fock, DFT, etc.). In our Unit we have carried out several SCR studies for several series of molecules and cell lines [25-34]. Here we present the results of a formal SCR study for a family of pyrimidine–benzimidazol hybrids recently published [35]. In addition to its intrinsic scientific value, this study will contribute to enlarge the data set necessary to build the abovementioned unified interaction model.

METHODS, MODELS AND CALCULATIONS

As the model-based method relating biological activity with electronic structure has been described in detail in a number of papers [34, 36-38], we present here only a short summary. The biological activity is a linear function of several local atomic reactivity indices (LARIs) and has the following form [39-43]:

$$\log(\mathrm{IC}_{50}) = a + bM_{D_i} + c\log\left[\sigma_{D_i}/(ABC)^{1/2}\right] + \sum_j \left[e_j Q_j + f_j S_j^E + s_j S_j^N\right] +$$
$$+ \sum_j \sum_m \left[h_j(m) F_j(m) + x_j(m) S_j^E(m)\right] + \sum_j \sum_{m'} \left[r_j(m') F_j(m') + t_j(m') S_j^N(m')\right] +$$
$$+ \sum_j \left[g_j \mu_j + k_j \eta_j + o_j \omega_j + z_j \varsigma_j + w_j Q_j^{\max}\right] + \sum_{K=1}^{U} O_K \qquad (1)$$

where M is the drug's mass, σ its symmetry number and ABC the product of the drug's moments of inertia about the three principal axes of rotation. Q_i is the net charge of atom j, S_j^E and S_j^N are, respectively, the total atomic electrophilic and nucleophilic superdelocalizabilities of atom j, $F_{j,m}$ ($F_{j,m'}$) is the Fukui index of the occupied (vacant) MO m (m') localized on atom j. $S_j^E(m)$ is the atomic electrophilic superdelocalizability of MO m localized on atom j, etc. The total atomic electrophilic superdelocalizability of atom j corresponds to the sum over occupied MOs of the $S_j^E(m)$'s and the total atomic nucleophilic superdelocalizability of atom j is the sum over vacant MOs of the $S_j^N(m)$'s. μ_j is the local atomic electronic chemical potential of atom j, η_j is the local atomic hardness of atom j, ω_j is the local atomic electrophilicity of atom j, ς_j is the local atomic softness

of atom j, and Q_j^{max} is the maximal amount of electronic charge that atom j may accept from another site. $HOMO_j$* refers to the highest occupied molecular orbital localized on atom j and $LUMO_j$* to the lowest empty MO localized on atom j.

They are called the local atomic frontier MOs. The O_K's are the orientational parameters of the substituents. The selected molecules are shown in Fig. 1 and Table 1. The experimental data selected for this study are the concentrations required to achieve the 50% inhibition of the tumor growth expressed as IC_{50} (cytotoxicity or inhibitory activity). This value is reported for four human cancer cell lines including MCF-7 (human breast cancer cell line), MGC-803 (human gastric cancer cell line), EC-9706 (human esophageal cancer cell line) and SMMC-7721 (human liver cancer cell line) using the MTT assay method. The IC50 (μM) values are listed in Table 1 [35].

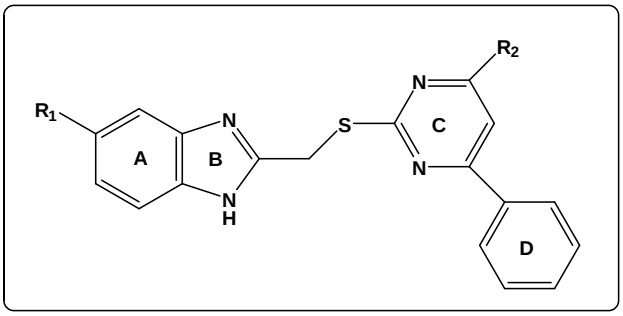

Figure 1: Structure of the pyrimidine–benzimidazol hybrids.

Table 1. Pyrimidine–benzimidazol hybrids and their biological activities.

Mol	R_1	R_2	log(IC_{50}) MCF-7	log(IC_{50}) MGC-803	log(IC_{50}) EC-9706	log(IC_{50}) SMMC-7721
1	H	OH	1.38	1.32	1.55	1.75
2	Cl	OH	1.36	1.29	1.51	1.73
3	H	Cl	1.01	0.99	1.38	1.48
4	Cl	Cl	0.85	0.91	1.37	1.45
5	H	4-Me-C_6H_4-NH	0.16	0.12	0.52	1.31
6	H	4-OMe-C_6H_4-NH	0.46	0.31	0.77	1.02
7	H	4-F-C_6H_4-NH	0.63	0.36	0.93	1.35
8	H	4-Cl-C_6H_4-NH	1.09	0.51	1.36	1.35
9	H	3-CF_3-C_6H_4-NH	0.88	0.58	0.98	1.46
10	H	2-OMe-C_6H_4-NH	--	1.66	--	--
11	H	C_6H_5-NH	0.75	0.79	1.00	1.50
12	H	3-Me-C_6H_4-NH	1.56	1.52	1.60	1.76
13	H	4-Bu-C_6H_4-NH	1.25	1.18	1.33	1.65
14	H	4-*i*-Pr-C_6H_4-NH	1.38	1.30	1.71	1.83
15	H	2-F-C_6H_4-NH	0.93	0.86	1.20	1.59
16	H	3-Cl-C_6H_4-NH	1.29	1.22	1.30	1.50
17	Cl	4-Me-C_6H_4-NH	0.15	0.03	0.45	1.29
18	Cl	4-OMe-C_6H_4-NH	0.29	0.03	0.57	1.11
19	Cl	4-F-C_6H_4-NH	0.80	0.63	1.34	1.15
20	Cl	4-Cl-C_6H_4-NH	1.02	0.64	1.19	1.31
21	Cl	3-CF_3-C_6H_4-NH	0.68	0.42	0.77	1.41
22	Cl	4-CH_3CH_2OCO-C_6H_4-NH	--	1.73	--	--

The electronic structure of all the molecules was calculated within DFT at the B3LYP/6-311g(d,p) level with the Gaussian program [44]. After full geometry optimization and single point calculations, all the numerical values for the electronic local atomic reactivity indices of Eq. 1 were calculated with the D-Cent-

QSAR software [45]. Negative electron populations coming from Mulliken Population Analysis were corrected as usual [46]. We made use of Linear Multiple Regression Analysis (LMRA) techniques to find the best solution of the system of equations 1 [47]. For each case (cell line), a matrix was built containing the logarithm of the dependent variable (IC_{50}) and the local atomic reactivity indices of all atoms of a common skeleton (defined as a set of atoms common to all molecules that accounts for virtually all the biological activity) as independent variables [37, 38]. The common skeleton numbering is shown in Fig. 2. The Statistica software was used for LMRA [47].

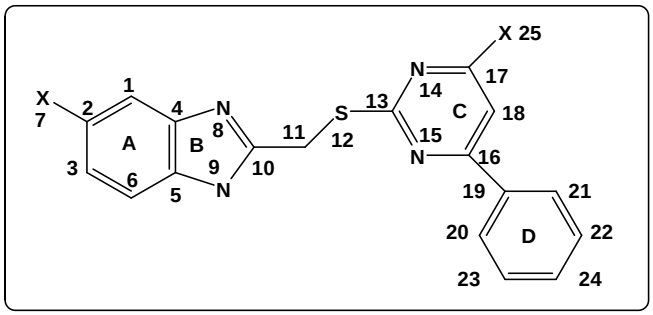

Figure 2. Common skeleton numbering.

RESULTS

Results for the SMMC-7721 cell line

The best equation obtained is:

$$\log(IC_{50}) = 1.50 - 0.07S_8^N(LUMO+1)^* - 0.11S_{10}^N(LUMO+2)^* + 3.35F_4(LUMO+2)^* - 0.40F_7(LUMO+2)^* + 2.89F_{15}(LUMO+2)^* - 0.27F_{24}(HOMO-2)^* \quad (2)$$

with n=20, R= 0.94, R^2= 0.88, adj. R^2= 0.82, F(6,13)=15.66 ($p<0.00003$) and a standard error of estimate of 0.09. No outliers were detected and no residuals fall outside the ±2σ limits. Here, $S_8^N(LUMO+1)^*$ is the orbital nucleophilic superdelocalizability of the second lowest vacant MO localized on atom 8, $S_{10}^N(LUMO+2)^*$ is the orbital nucleophilic superdelocalizability of the third lowest vacant MO localized on atom 10, $F_4(LUMO+2)^*$ is the Fukui index of the third lowest vacant MO localized on atom 4, $F_7(LUMO+2)^*$ is the Fukui index of the third lowest vacant MO localized on atom 7, $F_{15}(LUMO+2)^*$ is the Fukui index of the third lowest vacant MO localized on atom 15 and $F_{24}(HOMO-2)^*$ is the Fukui index of the third highest occupied MO localized on atom 24 (see Fig. 2 for atom numbering). Table 2 shows the beta coefficients and the results of the t-test for significance of coefficients. Table 3 displays the squared correlation coefficients for the variables appearing in Eq. 2, showing that there are no significant internal correlations. Fig. 3 displays the plot of observed *vs.* calculated log(IC_{50}) values. The associated statistical parameters of Eq. 2 indicate that this equation is statistically significant and that the variation of the numerical value of a group of six local atomic reactivity indices of atoms of the common skeleton explains about 82% of the variation of the inhibitory activity (cytotoxicity) against SMMC-7721 cells.

ISSN: 0975-8585

Table 2:Beta coefficients and *t*-test for significance of the coefficients in Eq. 2.

	Beta	t(13)	p-level
$S_8^N(LUMO+1)*$	-0.67	-6.63	<0.00002
$S_{10}^N(LUMO+2)*$	-0.44	-4.13	<0.001
$F_4(LUMO+2)*$	0.51	4.64	<0.0005
$F_7(LUMO+2)*$	-0.41	-3.52	<0.004
$F_{15}(LUMO+2)*$	0.38	3.49	<0.004
$F_{24}(HOMO-2)*$	-0.24	-2.21	<0.045

Table 3: Squared correlation coefficients for the variables appearing in Eq. 2.

	$S_8^N(LUMO+1)*$	$S_{10}^N(LUMO+2)*$	$F_4(LUMO+2)*$	$F_7(LUMO+2)*$	$F_{15}(LUMO+2)*$
$S_{10}^N(LUMO+2)*$	0.01	1.00			
$F_4(LUMO+2)*$	-0.02	0.10	1.00		
$F_7(LUMO+2)*$	-0.06	0.40	0.42	1.00	
$F_{15}(LUMO+2)*$	0.19	0.10	-0.19	-0.01	1.00
$F_{24}(HOMO-2)*$	-0.15	-0.00	-0.07	-0.07	0.34

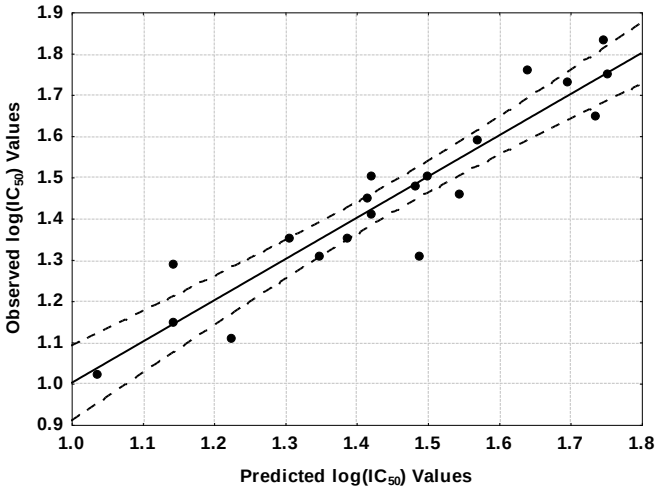

Figure 3: Observed *versus* calculated values (Eq. 2) of log (IC_{50}). Dashed lines denote the 95% confidence interval.

Results for the MGC-803 cell line.

A LMRA with all molecules detected one outlier. After deleting it, the best equation obtained is:

$$\log(IC_{50}) = 8.35 - 13.91F_{25}(LUMO+2)* + 2.12S_{12}^N(LUMO+2)* + 0.14S_{11}^N(LUMO+2)* + 4.54F_4(LUMO+2)* \quad (3)$$

with n=21, R= 0.87, R^2= 0.76, adj. R^2= 0.70, F(4,16)=12.48 (p<0.00009) and a standard error of estimate of 0.27. No outliers were detected and no residuals fall outside the ±2σ limits. Here, $F_{25}(LUMO+2)^*$ is the Fukui index of the third lowest vacant MO localized on atom 25, $S_{12}^N(LUMO+2)^*$ is the nucleophilic superdelocalizability of the third lowest vacant MO localized on atom 12, $S_{11}^N(LUMO+2)^*$ is the nucleophilic superdelocalizability of the third lowest vacant MO localized on atom 11 and $F_4(LUMO+2)^*$ is the Fukui index of the third lowest MO localized on atom 4 (see Fig. 2 for atom numbering). Table 4 shows the beta coefficients and the results of the t-test for significance of coefficients. Table 5 displays the squared correlation coefficients for the variables appearing in Eq. 3, showing that there are no significant internal correlations. Fig. 4 displays the plot of observed *vs.* calculated log(IC_{50}) values. The associated statistical parameters of Eq. 4 indicate that this equation is statistically significant and that the variation of the numerical value of a group of four local atomic reactivity indices of atoms of the common skeleton explains about 70% of the variation of the inhibitory activity against MGC-803 cells.

Table 4: Beta coefficients and *t*-test for significance of the coefficients in Eq. 3.

	Beta	t(16)	p-level
$F_{25}(LUMO+2)^*$	-0.79	-5.86	<0.00002
$S_{12}^N(LUMO+2)^*$	0.86	5.39	<0.00006
$S_{11}^N(LUMO+2)^*$	0.64	4.00	<0.001
$F_4(LUMO+2)^*$	0.31	2.46	<0.03

Table 5: Squared correlation coefficients for the variables appearing in Eq. 3.

	$F_{25}(LUMO+2)^*$	$S_{12}^N(LUMO+2)^*$	$S_{11}^N(LUMO+2)^*$
$S_{12}^N(LUMO+2)^*$	0.18	1.00	
$S_{11}^N(LUMO+2)^*$	0.18	-0.57	1.00
$F_4(LUMO+2)^*$	0.10	-0.12	0.13

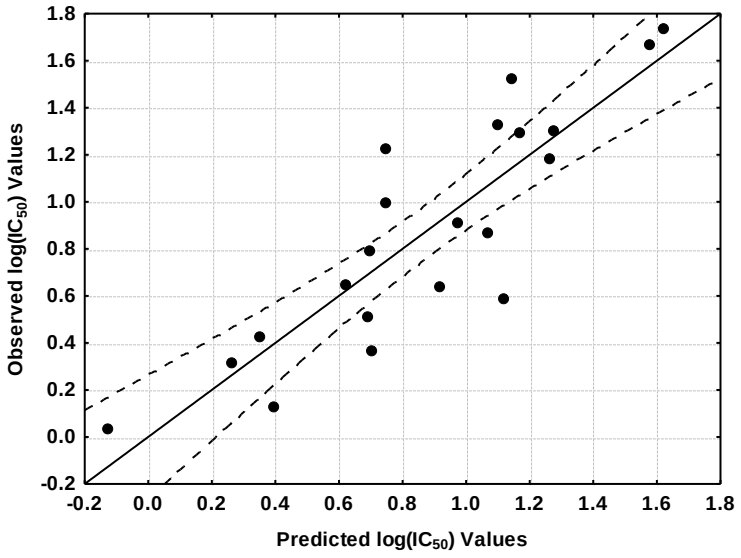

Figure 4: Observed *versus* calculated values (Eq. 3) of log (IC_{50}). Dashed lines denote the 95% confidence interval.

Results for the MCF-7 cell line.

The equation obtained is:

$$\log(IC_{50}) = 3.58 - 150.47F_{25}(LUMO)^* - 1.46F_5(LUMO+1)^* + 4.66F_{11}(LUMO+2)^* + 1.15S_7^E(HOMO-2)^* + 3.59F_{18}(LUMO+1)^* \quad (4)$$

with n=20, R= 0.92 R^2= 0.84, adj. R^2= 0.78, F(5,14)=14.55 (p<0.00004) and a standard error of estimate of 0.19. No outliers were detected and no residuals fall outside the ±2σ limits. Here, $F_{25}(LUMO)^*$ is the Fukui index of the lowest vacant MO localized on atom 25, $F_5(LUMO+1)^*$ is the Fukui index of the second lowest vacant MO localized on atom 5, $F_{11}(LUMO+2)^*$ is the Fukui index of the third lowest vacant MO localized on atom 11, $S_7^E(HOMO-2)^*$ is the electrophilic superdelocalizability of the third highest occupied MO localized on atom 7 and $F_{18}(LUMO+1)^*$ is the Fukui index of the second lowest vacant MO localized on atom 18 (see Fig. 2 for atom numbering).

Table 6 shows the beta coefficients and the results of the t-test for significance of coefficients. Table 7 displays the squared correlation coefficients for the variables appearing in Eq. 4, showing that there are no significant internal correlations. Fig. 5 displays the plot of observed *vs.* calculated log(IC_{50}) values. The associated statistical parameters of Eq. 4 indicate that this equation is statistically significant and that the variation of the numerical value of a group of five local atomic reactivity indices of atoms of the common skeleton explains about 78% of the variation of the inhibitory activity against MCF-7 cells.

Table 6: Beta coefficients and *t*-test for significance of the coefficients in Eq. 4.

	Beta	t(14)	p-level
$F_{25}(LUMO)^*$	-0.81	-7.01	<0.000006
$F_5(LUMO+1)^*$	-0.63	-5.35	<0.0001
$F_{11}(LUMO+2)^*$	0.75	5.34	<0.0001
$S_7^E(HOMO-2)^*$	0.40	3.48	<0.004
$F_{18}(LUMO+1)^*$	0.46	3.44	<0.004

Table 7: Squared correlation coefficients for the variables appearing in Eq. 4.

	$F_{25}(LUMO)^*$	$F_5(LUMO+1)^*$	$F_{11}(LUMO+2)^*$	$S_7^E(HOMO-2)^*$
$F_5(LUMO+1)^*$	-0.22	1.00		
$F_{11}(LUMO+2)^*$	0.09	0.21	1.00	
$S_7^E(HOMO-2)^*$	-0.04	0.22	-0.21	1.00
$F_{18}(LUMO+1)^*$	0.15	-0.11	-0.56	0.08

ISSN: 0975-8585

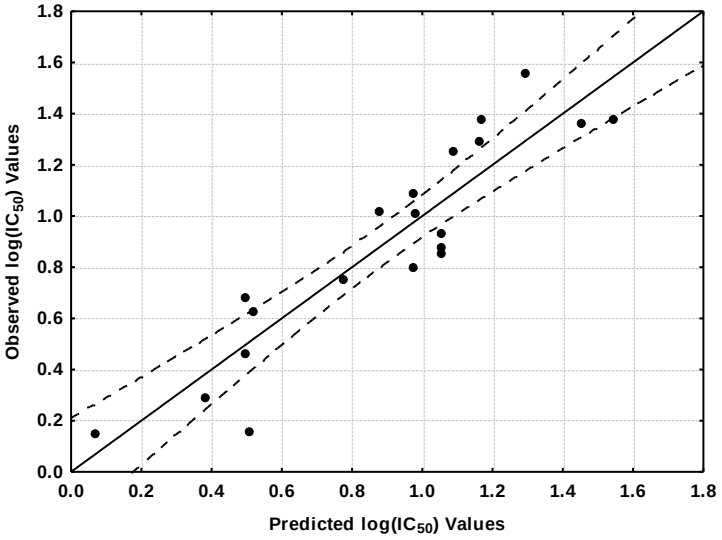

Figure 5: Observed *versus* calculated values (Eq. 4) of log (IC_{50}). Dashed lines denote the 95% confidence interval.

Results for the EC-9706 cell line:

No statistically significant equation was obtained for all the set. Extracting the molecule with the highest IC_{50} value (this way has worked well before) we obtained the following equation:

$$\log(IC_{50}) = 5.60 - 21.42 s_{14} - 0.14 S_{19}^{E}(HOMO-1)^{*} + 0.33 S_{2}^{E}(HOMO)^{*} + \\ + 7.20 F_{4}(LUMO+2)^{*} + 0.95 F_{20}(LUMO+2)^{*} + 0.73 F_{9}(HOMO)^{*} \quad (5)$$

with n=19, R= 0.97, R^2= 0.93, adj. R^2= 0.90, F(6,12)=27.77 (p<0.000001) and a standard error of estimate of 0.11. No outliers were detected and no residuals fall outside the ±2σ limits. Here, s_{14} is the local atomic softness of atom 14, $S_{19}^{E}(HOMO-1)^{*}$ is the Fukui index of the second highest occupied MO localized on atom 19, $S_{2}^{E}(HOMO)^{*}$ is the electrophilic superdelocalizability of the highest occupied MO localized on atom 2, $F_4(LUMO+2)^{*}$ is the Fukui index of the third lowest vacant MO localized on atom 4, $F_{20}(LUMO+2)^{*}$ is the Fukui index of the third lowest vacant MO localized on atom 20 and $F_9(HOMO)^{*}$ is the Fukui index of the highest occupied MO localized on atom 9 (see Fig. 2 for atom numbering).

Table 8: Beta coefficients and *t*-test for significance of the coefficients in Eq. 5.

	Beta	t(12)	p-level
s_{14}	-0.81	-8.49	<0.000002
$S_{19}^{E}(HOMO-1)^{*}$	-0.27	-3.26	<0.007
$S_{2}^{E}(HOMO)^{*}$	0.61	6.58	<0.00003
$F_4(LUMO+2)^{*}$	0.68	6.36	<0.00004
$F_{20}(LUMO+2)^{*}$	0.55	4.85	<0.0004
$F_9(HOMO)^{*}$	-0.26	-2.85	<0.01

ISSN: 0975-8585

Table 8 shows the beta coefficients and the results of the t-test for significance of coefficients. Table 9 displays the squared correlation coefficients for the variables appearing in Eq. 5, showing that there are no significant internal correlations. Fig. 6 displays the plot of observed *vs.* calculated log(IC_{50}) values. The associated statistical parameters of Eq. 5 indicate that this equation is statistically significant and that the variation of the numerical value of a group of five local atomic reactivity indices of atoms of the common skeleton explains about 90% of the variation of the inhibitory activity against EC-9706 cells.

Table 9: Squared correlation coefficients for the variables appearing in Eq. 5.

	S_{14}	$S_{19}^{E}(HOMO-1)^{*}$	$S_{2}^{E}(HOMO)^{*}$	$F_{4}(LUMO+2)^{*}$	$F_{20}(LUMO+2)^{*}$
$S_{19}^{E}(HOMO-1)^{*}$	0.15	1.00			
$S_{2}^{E}(HOMO)^{*}$	0.17	-0.24	1.00		
$F_{4}(LUMO+2)^{*}$	-0.19	0.13	-0.38	1.00	
$F_{20}(LUMO+2)^{*}$	0.56	-0.10	0.17	-0.50	1.00
$F_{9}(HOMO)^{*}$	0.14	0.18	0.20	0.24	0.14

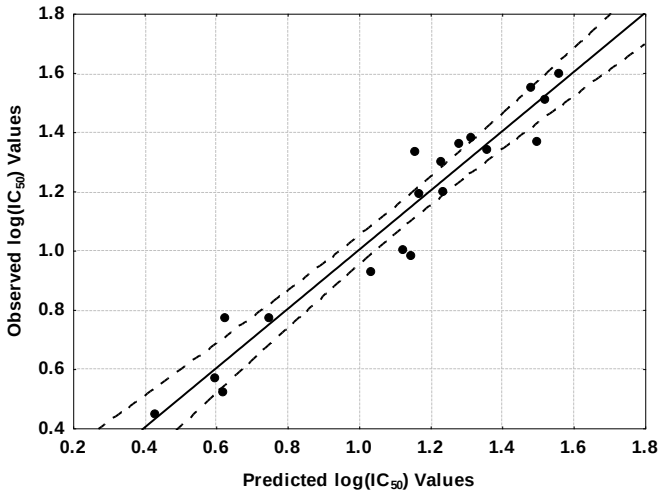

Figure 6. Observed *versus* calculated values (Eq. 5) of log (IC_{50}). Dashed lines denote the 95% confidence interval.

DISCUSSION

Molecular Electrostatic Potential (MEP):

Molecules that need to be recognized and guided to their action site(s) should have a qualitatively similar 3D MEP map. Figure 7 shows the MEP map of molecules 17 and 1 at 4.5 Å from the nuclei (with the fully optimized geometries) [48].

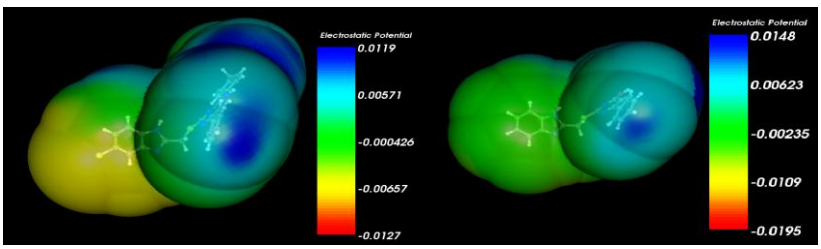

Figure 7. MEP map of molecules 17 (left) and 1 (right) at 4.5 Å of the nuclei.

We can see that there in both molecules the left side is surrounded by a negative MEP. The right side has a positive MEP region surrounding it. If we disregard the extra phenyl substituent of molecule 17, the remaining region has a qualitatively similar MEP distribution. We hypothesize that this area is the one facing the site for recognition and guidance. Figure 8 shows the MEP map of the same molecules for surfaces with isovalues of ±0.01 [49].

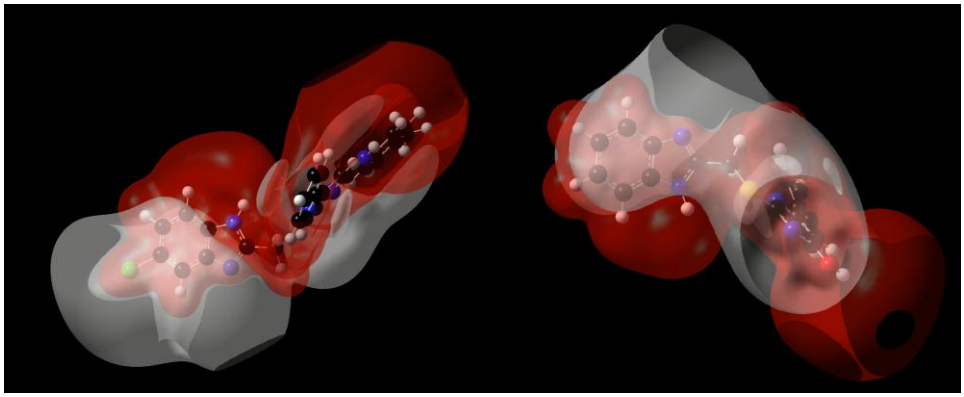

Figure 8. MEP map of molecules 17 (left) and 1 (right). The grey isovalue surface corresponds to negative MEP values (-0.01) and the reddish isovalue surface to positive MEP values (0.01).

We can see that, at the same isovalue, the MEP distribution is qualitatively similar around the A-B ring system. Because of the conformational flexibility of the rest of the molecule and our lack of knowledge of the conformation(s) adopted in the active site, it is very difficult to provide a sure statement about the role of MEP.

Conformational aspects

Molecule 17 is one of the most active in the series against all cell lines and molecule 1 one of the least active one. Figure 9 shows the ten lowest energy conformers of both molecules obtained with MarvinView and superimposed with Hyperchem (rings A and B were employed as a common element) [50, 51].

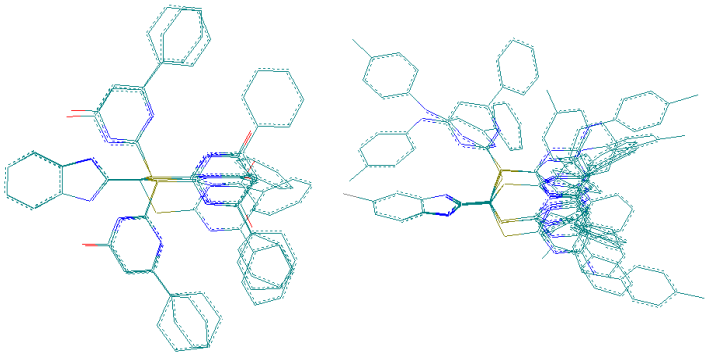

Figure 9. Superimposition of the ten lowest energy conformers of molecules 1 (left) and 17 (right).

We can see that both molecules have a high degree of conformational flexibility. Notice that in molecule 17 there are two conformers in which rings A-B engage in a π-π stacking interaction with other aromatic rings. In the case of molecule 1 there are four of such interactions. It is the (unknown) microscopic environment at the action site that will select one of these conformers as the active one.

ISSN: 0975-8585

Local Molecular Orbital Structure

Tables 10-13 show the local MO structure of atoms appearing in Eqs. 2-5 (the nomenclature is: Molecule (HOMO) / (HOMO-2)* (HOMO-1)* (HOMO)* - (LUMO)* (LUMO+1)* (LUMO+2)*, lp refers to a lone pair).

Table 10: Local Molecular Orbital Structure of atoms 2, 4, 5 and 7 of Pyrimidine–Benzimidazol Hybrids.

Mol	Mol.	Atom 2	Atom 4	Atom 5	Atom 7
3a	1 (87)	85π86π87π-90π93π94π	85π86π87π-90π91π93π	85π86π87π-93π94π96π	66σ73σ74σ-99σ100σ101σ
3b	2 (95)	93π94π95π-98π101π102π	93π94π95π-98π101π102π	93π94π95π-98π101π102π	93π94π95π-101π102π103σ
4a	3 (91)	89π90π91π-94π97π98π	89π90π91π-94π97π98π	89π90π91π-97π98π99π	76σ77σ78σ-103σ104σ105σ
4b	4 (99)	97π98π99π-102π105π106π	94σ98π99π-102π105π107π	97π98π99π-105π106π107π	97π98π99π-105π107π108σ
5a	5 (111)	108π109π110π-114π118π119π	108π109π110π-114π118π119π	108π109π110π-118π119π120π	91σ92σ94σ-126σ127σ131σ
5b	6 (115)	112π113π114π-118π122π123π	112π113π114π-118π122π123π	112π113π114π-122π123π124π	88σ96σ98σ-130σ132σ136σ
5c	7 (111)	109π110π111π-115π118π119π	109π110π111π-115π118π119π	109π110π111π-118π119π120π	92σ94σ96σ-126σ127σ130σ
5d	8 (115)	112π113π115π-119π122π123π	113π114π115π-119π122π123π	113π114π115π-122π123π124π	89σ96σ98σ-130σ131σ135σ
5e	9 (123)	121π122π123π-127π130π131π	121π122π123π-127π131π132π	121π122π123π-130π131π132π	105σ106σ108σ-137σ138σ139σ
5f	10 (115)	112π113π114π-118π122π123π	112π113π114π-118π122π124π	112π113π114π-122π123π124π	95σ96σ98σ-130σ131σ132σ
5h	11 (107)	105π106π107π-110π114π115π	105π106π107π-110π114π115π	105π106π107π-114π115π116π	88σ89σ92σ-122σ123σ126σ
5i	12 (111)	109π110π111π-114π118π119π	109π110π111π-114π118π120π	109π110π111π-118π119π120π	91σ92σ94σ-126σ127σ131σ
5j	13 (123)	120π121π122π-126π130π131π	120π121π122π-126π130π132π	120π121π122π-130π131π132π	101σ103σ104σ-138σ140σ145σ
5k	14 (119)	116π117π118π-122π126π127π	116π117π118π-122π126π128π	116π117π118π-126π127π128π	90σ97σ101σ-134σ135σ136σ
5l	15 (111)	108π109π111π-114π118π119π	109π110π111π-114π118π119π	108π109π111π-118π119π120π	93σ94σ96σ-126σ127σ130σ
5m	16 (115)	113π114π115π-119π122π123π	113π114π115π-119π122π123π	113π114π115π-122π123π124π	89σ96σ98σ-130σ131σ132σ
6a	17 (119)	116π117π118π-122π126π127π	116π117π118π-122π126π127π	116π117π118π-122π126π127π	116π117π118π-126π128π129σ
6b	18 (123)	120π121π122π-126π130π131π	120π121π122π-126π130π131π	120π121π122π-126π130π131π	120π121π122π-130π131π133σ
6c	19 (119)	117π118π119π-122π126π127π	116π117π118π-122π126π127π	117π118π119π-126π127π129π	116π117π118π-126π129σ130σ
6d	20 (123)	121π122π123π-126π130π131π	121π122π123π-126π130π132π	121π122π123π-130π132π134π	121π122π123π-130π132π134σ
6e	21 (131)	129π130π131π-135π138π139π	128π129π131π-135π138π140π	129π130π131π-135π138π140π	129π130π131π-138π140π141σ
6f	22 (123)	120π121π122π-126π130π131π	120π121π122π-126π130π131π	120π121π122π-126π130π134π	120π121π122π-130π132σ133σ

ISSN: 0975-8585

Table 11: Local Molecular Orbital Structure of atoms 8-11 of Pyrimidine–Benzimidazol Hybrids.

Mol	Mol.	Atom 8	Atom 9	Atom 10	Atom 11
3a	1 (87)	83σ86π87π-90π91π95π	79π82σ86π-90π91π93π	85π86π87π-90π91π93π	82σ85σ87σ-90σ91σ93σ
3b	2 (95)	89σ90σ94π-97π98π102π	90σ94π95π-98π101π103π	93π94π95π-97π98π101π	90σ93σ95σ-98σ101σ102σ
4a	3 (91)	87σ90π91π-94π99π100π	86π90π91π-94π97π98π	89π90π91π-94π98π99π	86σ89σ91σ-94σ97σ98σ
4b	4 (99)	93σ94σ98π-102π107π108π	94π98π99π-102π105π106π	97σ98π99π-102π105π107π	92σ94σ97σ-102σ105σ106σ
5a	5 (111)	105σ109π110π-114π120π121π	103σ104σ109π-114π118π119π	108π109π110π-114π118π120π	104σ108σ110σ-114σ118σ119σ
5b	6 (115)	109σ113π114π-118π125π126π	107π108σ113π-118π122π123π	112σ113π114π-118π122π125π	108σ112σ114σ-118σ122σ123σ
5c	7 (111)	106σ109π110π-115π120π121π	103π104π109π-115π118π119π	109π110π111π-115π118π120π	104σ108σ110σ-115σ118σ120σ
5d	8 (115)	113π114π115π-119π126π127π	109σ113π114π-119π122π123π	113π114π115π-119π123π125π	109σ112σ115σ-119σ122σ123σ
5e	9 (123)	118σ122π123π-127π13π2133π	117σ121π122π-127π131π132π	120σ121π123π-127π131π132π	117σ120σ123σ-127σ130σ131σ
5f	10 (115)	109σ113π114π-118π124π125π	107σ108σ113π-118π122π124π	108σ112π114π-118π122π124π	108σ112σ114σ-118σ122σ123σ
5h	11 (107)	105π106π107π-110π116π117π	100σ105π106π-110π114π115π	105π106π107π-110π114π116π	97σ100σ104σ-110σ114σ116σ
5i	12 (111)	105σ109π110π-114π120π121π	103σ104σ109π-114π118π119π	109π110π111π-114π118π120π	104σ108σ110σ-114σ118σ120σ
5j	13 (123)	117σ121π122π-126π132π133	115σ116σ121π-126π130π131π	120π121π122π-126π130π132π	116σ120σ122σ-126σ130σ132σ
5k	14 (119)	113σ117π118π-122π128π129π	111σ112σ117π-122π126π128π	116σ117π118π-122π126π128π	112σ116σ118σ-122σ126σ128σ
5l	15 (111)	109π110π111π-114π120π121π	104σ109π110π-114π118π119π	109π110π111π-114π118π120π	104σ108π111σ-114σ118σ120σ
5m	16 (115)	113π114π115π-119π125π126π	108σ113π114π-119π122π123π	112π113115π-119π120π123π	108σ112σ115σ-119σ122σ123σ
6a	17 (119)	111σ112σ117π-122π127π128π	111σ117π118π-122π126π129π	116π117π118π-121π122π126π	112σ116σ118σ-122σ126σ127σ
6b	18 (123)	115σ116σ121π-126π131π133π	115σ121π122π-126π130π133π	120π121π122π-125π126π130π	116σ120σ122σ-126σ130σ131σ
6c	19 (119)	111σ112σ117π-122π127π128π	111σ117π118π-122π126π129π	116π117π118π-121π122π126π	112σ116σ118σ-122σ126σ127σ
6d	20 (123)	115σ116σ121π-126π132π134π	121π122π123π-126π130π134π	121π122π123π-126π130π134π	111σ116σ120σ-126σ130σ131σ
6e	21 (131)	125σ129π130π-135π140π141π	129π130π131π-135π138π141π	128π129π131π-135π138π141π	125σ128σ131σ-135σ138σ139σ
6f	22 (123)	115σ116σ121π-126π131π132π	115σ121π122π-126π130π134π	120π121π122π-125π126π130π	115σ116σ122σ-126σ130σ131σ

ISSN: 0975-8585

Table 12: Local Molecular Orbital Structure of atoms 12, 14, 15 and 18 of Pyrimidine–Benzimidazol Hybrids.

Mol	Mol.	Atom 12	Atom 14	Atom 15	Atom 18
3a	1 (87)	85π86π87lp-88lp89lp90σ	83σ84π85π-88π89π92π	84π85π87π-88π89π91π	83σ84π85π-88π89π91π
3b	2 (95)	93π94lp95lp-96lp97lp98σ	91σ92π93π-96π97π100π	92π93π95π-96π97π98π	92π93π95π-96π97π98π
4a	3 (91)	89lp90lp91lp-93lp94σ96lp	87σ88π89π-92π93π96π	87σ88π89π-92π93π 95π	85σ88π89π-92π93π95π
4b	4 (99)	97lp98lp99lp-101lp102lp104lp	95π96π97π-100π101π104π	95π96π97π-100π101π103π	94σ96π97π-100π101π103π
5a	5 (111)	109lp110lp111lp-112lp113lp114σ	109π110π111π-112π113π117π	108π110π111π-112π113π115π	106π108π111π-112π113π115π
5b	6 (115)	112lp113lp114lp-116lp117lp118σ	111π112π115π-116π117π121π	112π114π115π-116π117π119π	111π112π115π-116π117π119π
5c	7 (111)	109lp110lp111lp-112lp113lp115σ	109π110π111π-112π113π117π	107π108π111π-112π113π116π	107π108π111π-112π113π116π
5d	8 (115)	113lp114lp115lp-117lp119σ121lp	112π113π114π-116π117π121π	112π114π115π-116π117π121π	112π114π115π-116π117π120π
5e	9 (123)	121lp122π123lp-125lp127σ129lp	119π120π121π-124π125π129π	121π122π123π-124π125π126π	121π122π123π-124π125π126π
5f	10 (115)	113π114lp115lp-117lp118σ121lp	112π114π115π-116π117π121π	112π114π115π-116π117π119π	110π112π115π-116π117π119π
5h	11 (107)	105lp106σ107lp-108lp109lp110σ	105π106π107π-108π109π113π	104π106π107π-108π109π111π	104π106π107π-108π109π111π
5i	12 (111)	109lp110lp111lp-112lp113lp114σ	109π110π111π-112π113π117π	106π108π111π-112π113π115π	106π108π111π-112π113π115π
5j	13 (123)	121lp122lp123lp-124lp125lp126σ	120π122π123π-124π125π129π	120π122π123π-124π125π127π	118π120π123π-124π125π127π
5k	14 (119)	117lp118lp119lp-120lp121lp122σ	117π118π119π-120π121π125π	115π116π119π-120π121π123π	114π116π119π-120π121π123π
5l	15 (111)	109lp110lp111lp-113lp114σ117lp	108π109π110π-112π113π117π	108π110π111π-112π113π117π	108π110π111π-112π113π115π
5m	16 (115)	113lp114π115lp-117lp119σ121lp	111π112π113π-116π117π121π	113π114π115π-116π117π121π	113π114π115π-116π117π120π
6a	17 (119)	117lp118lp119π-120lp121lp122σ	116π118π119π-120π121π125π	115π116π119π-120π121π123π	114π116π119π-120π121π122π
6b	18 (123)	120π121lp122lp-124lp125lp126σ	120π122π123π-124π125π129π	120π122π123π-124π125π126π	120π122π123π-124π125π126π
6c	19 (119)	117lp118lp119lp-120lp121lp122σ	116π118π119π-120π121π125π	115π116π119π-120π121π124π	115π116π119π-120π121π124π
6d	20 (123)	121lp122lp123lp-125lp126σ129lp	120π122π123π-124π125π129π	119π120π123π-124π125π129π	119π120π123π-124π125π128π
6e	21 (131)	129σ130π131lp-133lp135σ137lp	127π128π130π-132π133π137π	127π130π131π-132π133π137π	128π130π131π-132π133π136π
6f	22 (123)	121lp122lp123lp-125lp126σ129lp	120π122π123π-124π125π129π	120π122π123π-124π125π127π	119π120π123π-124π125π126π

ISSN: 0975-8585

Table 13: Local Molecular Orbital Structure of atoms 19, 20, 24 and 25 of Pyrimidine–Benzimidazol Hybrids.

Mol	Mol.	Atom 19	Atom 20	Atom 24	Atom 25
3a	1 (87)	83π84π85π-88π92π100σ	83π84π85π-88π89π90π	83π84π85π-88π92π97σ	80π81π85π-88π89π91π
3b	2 (95)	91π92π93π-96π99π100π	91π92π93π-96π97π99π	91π92π93π-96π99π100π	89σ90σ93π-96π97π100π
4a	3 (91)	87π88π89π-92π95π96π	87π88π89π-92π95π96π	87π88π89π-92π95π96π	84π85σ89π-92π93π96π
4b	4 (99)	95π96π97π-100π103π104π	95π96π97π-100π103π104π	95π96π97π-100π103π104π	92π93π97π-100π101π104π
5a	5 (111)	106π107π108π-112π115π116π	106π107π108π-112π113π115π	107π108π111π-112π115π116π	102π108π111π-112π113π117π
5b	6 (115)	110π111π112π-116π119π120π	110π111π112π-116π117π119π	109π111π112π-116π119π120π	103π106π115π-116π117π123π
5c	7 (111)	106π107π108π-112π116π117π	106π107π108π-112π113π116π	107π108π111π-112π116π117π	108π110π111π-112π113π117π
5d	8 (115)	110π111π112π-116π120π121π	110π111π112π-116π117π120π	110π111π112π-116π120π121π	113π114π115π-116π117π121π
5e	9 (123)	119π120π121π-124π128129π	118π119π120π-124π128π130π	119π120π121π-124π128π129π	120π121π122π-124π125π129π
5f	10 (115)	109π110π112π-116π119π120π	109π110π112π-116π117π119π	109π110π112π-116π119π120π	106π111π115π-116π117π121π
5h	11 (107)	102π103π104π-108π111π112π	102π103π104π-108π109π111π	103π104π107π-108π111π112π	105π106π107π-108π109π113π
5i	12 (111)	105π106π108π-112π115π116π	105π106π108π-112π113π115π	106π108π111π-112π115π116π	108π110π111π-112π113π117π
5j	13 (123)	118π119π120π-124π127π128π	118π119π120π-124π125π127π	119π120π123π-124π127π128π	111π114π123π-124π125π129π
5k	14 (119)	114π115π116π-120π123π124π	114π115π116π-120π121π123π	115π116π119π-120π123π124π	110π116π119π-120π121π125π
5l	15 (111)	106π107π108π-112π115π117π	106π107π108π-112π113π115π	107π108π110π-112π115π117π	109π110π111π-112π113π117π
5m	16 (115)	109π110π112π-116π120π121π	109π110π112π-116π119π120π	110π112π113π-116π120π121π	112π113π114π-116π117π121π
6a	17 (119)	114π115π116π-120π123π124π	114π115π116π-120π121π123π	115π116π119π-120π123π124π	110π112σ119π-120π121π125π
6b	18 (123)	118π119π120π-124π127π128π	117π119π120π-124π125π127π	118π119π120π-124π127π128π	115π116σ123π-124π125π132π
6c	19 (119)	114π115π116π-120π124π125π	114π115π116π-120π121π124π	115π116π119π-120π124π125π	116π118π119π-120π121π125π
6d	20 (123)	118π119π120π-124π128π129π	118π119π120π-124π128π131π	119π120π123π-124π128π129π	120π122π123π-124π125π129π
6e	21 (131)	127π128π130π-132π133π136π	126π127π128π-132π136π139π	127π128π130π-132π133π136π	128π129π130π-132π133π137π
6f	22 (123)	117π118π120π-124π127π128π	117π118π120π-124π125π127π	118π119π120π-124π127π128π	116σ119π123π-124π125π129π

SMMC-7721 cell line:

The beta values (Table 2) indicate that the importance of the variables is $S_8^N(LUMO+1)^*$ > $F_4(LUMO+2)^*$ > $S_{10}^N(LUMO+2)^*$ = $F_7(LUMO+2)^*$ > $F_{15}(LUMO+2)^*$ > $F_{24}(HOMO-2)^*$. A variable-by-variable (VbV) analysis of Eq. 2 indicates that a high inhibitory activity is associated with high values for $F_7(LUMO+2)^*$ and $F_{24}(HOMO-2)^*$; and with small values for

$F_4(LUMO+2)*$ and $F_{15}(LUMO+2)*$. A high value for $F_7(LUMO+2)*$ ($(LUMO+2)_7^*$ is a σ MO, Table 10, sixth column) suggests that atom 7 (an H or Cl substituent in ring A) should be interacting with an electron-rich center (see Fig. 2). In the case of hydrogen, we can be in the presence of a favorable weak π-σ interaction between C-H and a π ring system. In the case of chlorine the interaction can be of the halogen kind. It is very important to notice the change of the local MO structure when replacing a hydrogen atom by a chlorine one: the two frontier local MOs are of σ nature in the former and of π nature in the latter (Table 10, sixth column). Another important point to mention is that in the case of the H substituent, its local frontier MOs are very far from the molecule's one. In the case of the Cl substituent the local HOMO* is almost coincident with the molecular HOMO, while the local LUMO* approaches the molecule's LUMO. Finally, the fact that $(LUMO+2)_7^*$ interacts implies that $(LUMO+1)_7^*$ and $(LUMO)_7^*$ are also participating in the interaction. A high value for $F_{24}(HOMO-2)*$ ($(HOMO-2)_{24}^*$ is a π MO, Table 13, fifth column) suggests that atom 24 is interacting with an electron-deficient center through its first three highest occupied MOs. This interaction could be of the type π-cation, π-π or π-amide one. $(LUMO+2)_4^*$, $(LUMO+1)_4^*$ and $(LUMO)_4^*$ are π MOs in all molecules (Table 10, fourth column). A small value for $F_4(LUMO+2)*$ is interpreted as follows. $(LUMO)_4^*$ and $(LUMO+1)_4^*$ interact in a favorable manner with an electron-rich center. The kind of interaction could be π-π, π-anion, π-lone pair or π-σ. This interaction could be weakened by an unfavorable interaction of $(LUMO+2)_4^*$ with the vacant frontier local MO of the counterpart [52, 53]. $(LUMO+2)_{15}^*$ is a π MO in all molecules (Table 12, fifth column).

A small value for $F_{15}(LUMO+2)*$ can be interpreted exactly as the previous case: an interaction of atom 15 with an electron-rich center through its first two lowest vacant MOs and a modulation of this interaction by an unfavorable one of $(LUMO+2)_{15}^*$ with the vacant frontier local MO of the counterpart. $(LUMO+1)_8^*$ is a π MO (Table 11, third column). As $S_8^N(LUMO+1)*$ is a positive number, a high value for is associated with a high inhibitory activity. Therefore it is suggested that atom 8 (see Fig. 2) is interacting with an electron-rich center through its first two lowest vacant MOs. $(LUMO+2)_{10}^*$ is a π MO (Table 11, fifth column). A high value for $S_{10}^N(LUMO+2)*$ is required for a high inhibitory activity. Interpreting this as in the prior case, atom 10 (see Fig. 2) is interacting with electron-rich center through its first three lowest vacant MOs. These two interactions can be of π-π, π-anion, π-donor or π-lone pair kinds. All these suggestions are presented in the two-dimensional (2D) partial pharmacophore of Fig. 10. If atoms 4, 8 and 10 have a common interaction site, it could be a π ring system.

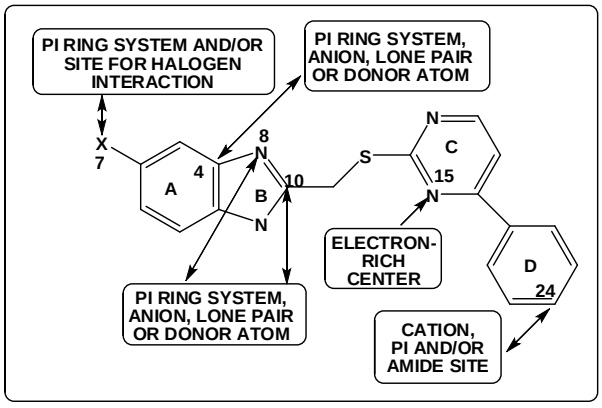

Figure 10. Partial 2D pharmacophore for the variation of the inhibitory activity against SMMC-7721 cells (Eq. 2).

ISSN: 0975-8585

MGC-803 cell line:

The beta values (Table 4) indicate that the importance of the variables is $S_{12}^{N}(LUMO+2)^*$ > $F_{25}(LUMO+2)^*$ > $S_{11}^{N}(LUMO+2)^*$ > $F_4(LUMO+2)^*$. A VbV analysis of Eq. 3 shows that a high inhibitory activity is associated with high values for $F_{25}(LUMO+2)^*$ and with small values for $F_4(LUMO+2)^*$. In the case of the nucleophilic superdelocalizabilities, the constants associated to them in Eq. 3 are positive. They will be analyzed below. $(LUMO+2)_{25}^{*}$ is a π MO (Table 13, sixth column). A high value for this reactivity index strongly suggests that atom 25 is interacting favorably with an electron-rich center through its three lowest vacant MOs. Atom 25 is nitrogen (in the majority of cases), oxygen or chlorine (Table 1). This interaction could be with an anion or with a lone pair.

is a π MO (Table 10, fourth column). A small value for $F_4(LUMO+2)^*$ can be interpreted as an unfavorable interaction of $(LUMO+2)_4^*$ with vacant MOs of a counterpart. The favorable interaction occurs through the first two lowest vacant MOs of atom 4 and an electron-rich center (a π system, an anion, a lone pair, a donor atom). $(LUMO+2)_{11}^{*}$ is a σ MO (all local MOs are of σ nature in atom 11). A low value for $S_{11}^{N}(LUMO+2)^*$ suggests an unfavorable interaction with other vacant σ MOs [52, 53]. Then atom 11 seems to interact with a rich σ-electron system through its two lowest vacant MOs. Good candidates for these interactions are CH_2 groups and π systems for example.

$(LUMO+2)_{12}^{*}$ is a lone pair or a σ MO (Table 12, third column). A low value for $S_{12}^{N}(LUMO+2)^*$ is interpreted by suggesting that $(LUMO)_{12}^{*}$ and $(LUMO+1)_{12}^{*}$ MOs (of σ or lone pair nature) are interacting in a favorable way with a rich-electron counterpart. This interaction seems to be weakened by an unfavorable interaction of $(LUMO+2)_{12}^{*}$ with empty MOs of a moiety of the site. A very important fact to mention is that, as atoms 11 and 12 are bonded, they seem to interact with a common site. All these suggestions are displayed in the 2D partial pharmacophore shown in Fig. 11.

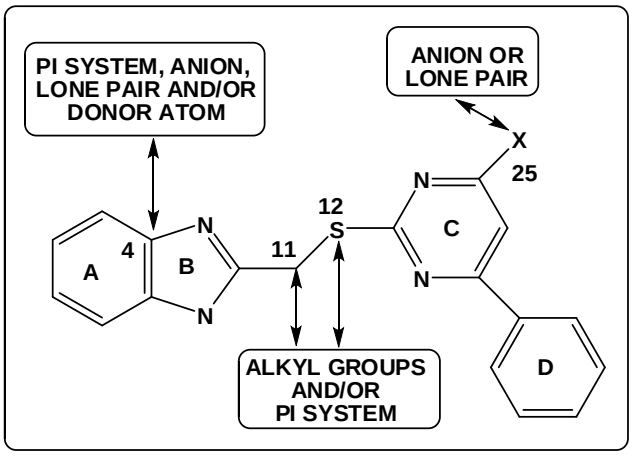

Figure 11. Partial 2D pharmacophore for the variation of the inhibitory activity against MGC-803 cells (Eq. 3).

MCF-7 cell line:

The beta values (Table 6) indicate that the importance of the variables is $F_{25}(LUMO)^*$> $F_{11}(LUMO+2)^*$ > $F_5(LUMO+1)^*$> $F_{18}(LUMO+1)^*$ > $S_7^E(HOMO-2)^*$. A VbV analysis of Eq. 4 shows that a high inhibitory activity is associated with high values for $F_{25}(LUMO)^*$, $F_5(LUMO+1)^*$

and $S_7^E(HOMO-2)*$; and with small values for $F_{18}(LUMO+1)*$ and $F_{11}(LUMO+2)*$. A high value for $F_{25}(LUMO)*$ can be interpreted in the same way than for the case of the MGC-803 cell line: atom 25 is interacting with an anion or with a lone pair through its lowest vacant MO. A high value for $F_5(LUMO+1)*$ suggests that atom 5 is interacting with an electron-rich center through its two lowest vacant MOs. As in the case of the SMMC-7721 cell line, these interactions can be of π-π, π-anion, π-donor or π-lone pair nature. Atom 7, as we said before, is the atom bonded to atom 2 of ring A (see Fig. 2). $(LUMO+2)_{11}^*$ is a σ MO in all molecules. A low value for $F_{11}(LUMO+2)*$ suggests a limiting unfavorable interaction of $(LUMO+2)_{11}^*$ with empty (σ) MOs. Atom 11 interacts with a moiety containing occupied σ MOs only through its first two lowest vacant MOs. $(HOMO-2)_7^*$ is a σ MO in 14 molecules and a π MO in 8 molecules (Table 10, sixth column). Given that the associated p value is too high (Table 6) we shall not propose an interaction mechanism. This also holds for $F_{18}(LUMO+1)*$. All the above suggestions are displayed in the 2D partial pharmacophore shown in Fig. 12.

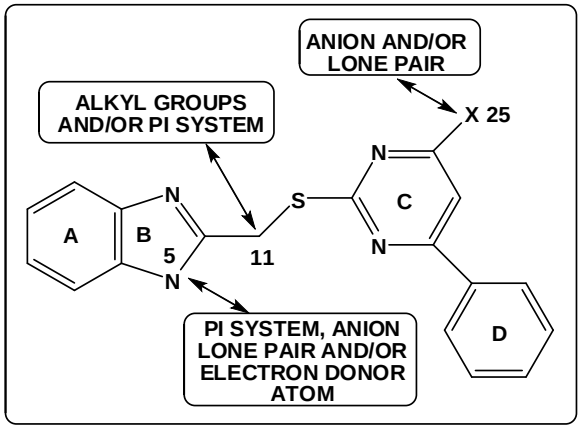

Figure 12. Partial 2D pharmacophore for the variation of the inhibitory activity against MCF-7 cells (Eq. 4).

EC-9706 cell line:

The beta values (Table 8) indicate that the importance of the variables is s_{14} > $F_4(LUMO+2)*$ > $S_2^E(HOMO)*$ > $F_{20}(LUMO+2)*$ > $S_{19}^E(HOMO-1)*$ > $F_9(HOMO)*$. A VbV analysis of Eq. 5 shows that a high inhibitory activity is associated with high values for s_{14}, $S_{19}^E(HOMO-1)*$ and $S_2^E(HOMO)*$; and with small values for $F_4(LUMO+2)*$ and $F_{20}(LUMO+2)*$. $F_9(HOMO)*$ will not be discussed due to its high p value (Table 8). s_{14} is the local atomic softness of atom 14 and it is defined as the inverse of the $(HOMO)_{14}^*$-$(LUMO)_{14}^*$ energy gap. A high value for s_{14} is obtained by diminishing that gap. An examination of Fig. 2 suggests that, in this case, this can be achieved by an appropriate substitution on position 18 or, if rings C and D are coplanar, by substitutions on atoms 20-24. As s_{14} is a number (i.e., it is not associated with a specific MO) we can make only an educated guess about the kind of interactions of this atom. In all molecules the frontier local MOs are of π nature. Atom 14 has a negative net charge. If atom 14 is interacting with a moiety through its $(HOMO)_{14}^*$, it can do it with another π system, with a cation or with an electron-accepting atom. If it uses its $(LUMO)_{14}^*$, it can possibly interact with an anion, a lone pair, a π system or an electron-donor atom. $(HOMO-1)_{19}^*$ is a π MO in all molecules (Table 13, third column). A high value for $S_{19}^E(HOMO-1)*$ indicates that atom 19 is interacting with an electron-deficient center through its first two occupied local MOs. This interaction could be with another π system, with a cation or with an

electron-acceptor atom. $(HOMO)_2^*$ is a π MO (Table 10, third column). A high value for $S_2^E(HOMO)*$ suggests that atom 2 is interacting with an electron-deficient center through its first occupied local MO. The kinds of interactions are similar to the ones proposed for atom 19. $(LUMO+2)_4^*$ is a π MO (Table 10, fourth column). A small value for $F_4(LUMO+2)*$ suggests an unfavorable interaction of this MO with vacant MOs of a moiety that weakens the favorable interaction of $(LUMO)_4^*$ and $(LUMO+1)_4^*$ with an electron-rich center. A similar analysis is applicable to $F_{20}(LUMO+2)*$. The corresponding 2D partial pharmacophore is shown in Fig. 13.

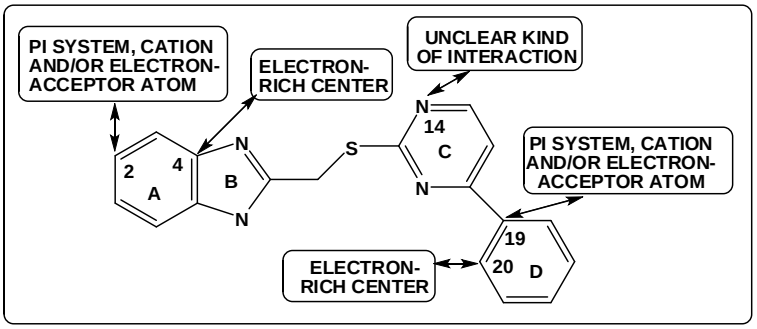

Figure 13. Partial 2D pharmacophore for the variation of the inhibitory activity against EC-9706 cells (Eq. 5).

About the nature of the common skeleton:

The common skeleton is a theoretical construct allowing us to detect atoms involved in the interactions with a site. As such, it is dependent on the composition of the set of molecules and the choice of the scientist. For example, in a recent study of the relationships between electronic structure and cytotoxicity of a group of N^2-alkylated quaternary β-carbolines against several tumoral cell lines, it was not possible to obtain a common skeleton for all the set [33]. In the case presented here, the observation of Figs. 3-6 shows that too many points are relatively far from the 90% confidence interval.

On the other hand, the percentage of explanation of Eqs. 2-4 is very low. Disregarding any explanation involving the quality of the experimental results, the abovementioned facts point to the possibility that some molecules have extra interaction sites that are not included in the common skeleton. The examination of Table 1 shows that eighteen molecules have a NH-phenyl moiety. Therefore, we built a new set excluding molecules 1-4 and expanded the common skeleton with ring E as shown in Fig. 14.

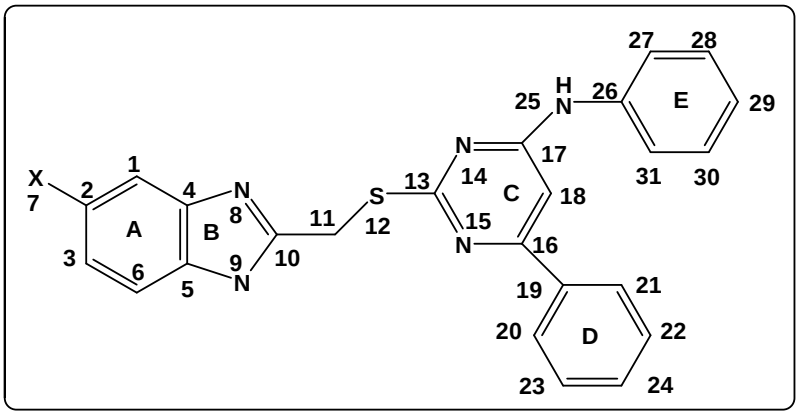

Figure 14. Enlarged common skeleton for the pyrimidine–benzimidazol hybrids.

The results obtained for the enlarged common skeleton are as follows:

SMMC-7721 cell line:

The best equation is:

$$\log(IC_{50}) = -2.04 + 0.62\eta_{30} - 0.52S_{26}^{E}(HOMO-2)^{*} - 0.01S_{3}^{N}(LUMO+1)^{*} + 0.56F_{30}(LUMO+1)^{*} + 0.59F_{7}(HOMO-1)^{*} \quad (6)$$

with n=16, R= 0.98, R^2= 0.97, adj. R^2= 0.95, F(5,10)=61.48 (p<0.000001) and a standard error of estimate of 0.05. No outliers were detected and no residuals fall outside the ±2σ limits. No significant correlation exists among independent variables. Here, η_{30} is the local hardness of atom 30, $S_{26}^{E}(HOMO-2)^{*}$ is the nucleophilic superdelocalizability of the third highest occupied MO localized on atom 26, $S_{3}^{N}(LUMO+1)^{*}$ is the nucleophilic superdelocalizability of the second lowest vacant MO localized on atom 3, $F_{30}(LUMO+1)^{*}$ is the Fukui index of the second lowest vacant MO localized on atom 30 and $F_{7}(HOMO-1)^{*}$ is the Fukui index of the second highest MO localized on atom 7. This equation is statistically significant and the variation of the numerical value of a group of five local atomic reactivity indices of atoms of the common skeleton explains about 95% of the variation of the inhibitory activity. Fig. 15 displays the plot of observed *vs.* calculated log(IC_{50}) values.

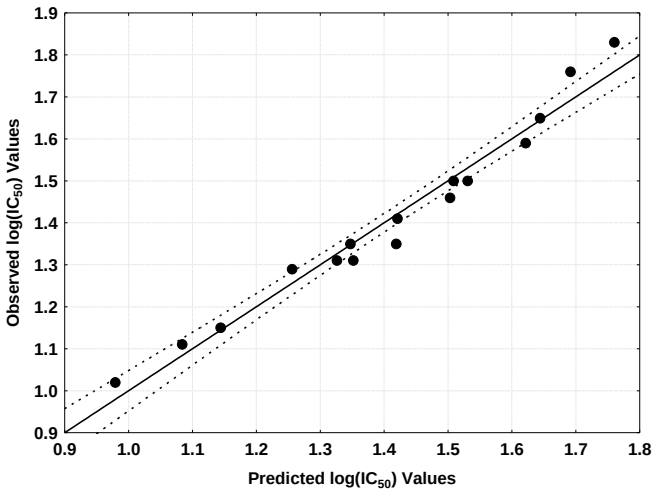

Figure 15. Observed *versus* calculated values (Eq. 6) of log (IC_{50}). Dashed lines denote the 95% confidence interval.

We can see that now nearly all points lie inside or close to the confidence interval. Beta values (not shown) indicate that the importance of variables is η_{30} >> $S_{26}^{E}(HOMO-2)^{*}$ = $S_{3}^{N}(LUMO+1)^{*}$ > $F_{30}(LUMO+1)^{*}$ > $F_{7}(HOMO-1)^{*}$. A high inhibitory activity is associated with low values for η_{30}, $S_{26}^{E}(HOMO-2)^{*}$, $F_{30}(LUMO+1)^{*}$ and $F_{7}(HOMO-1)^{*}$; and with a $(LUMO+1)_{3}^{*}$ MO available for interactions. η_{30} is the $(HOMO)_{30}^{*}$ - $(LUMO)_{30}^{*}$ distance (the local atomic hardness). A small value can be obtained by shifting upwards the $(HOMO)_{30}^{*}$ energy, by shifting downwards the $(LUMO)_{30}^{*}$ energy or by both procedures. As η_{30} is a number, the nature of the interaction of atom 30 with a counterpart cannot be established for the moment. Table 14 shows the local molecular orbital structure of atoms 26-28 and 30.

ISSN: 0975-8585

Table 14. Local Molecular Orbital Structure of atoms 26-28 and 30 of Pyrimidine–Benzimidazol Hybrids.

Mol	Mol.	Atom 26	Atom 27	Atom 28	Atom 30
5a	5 (111)	77σ80σ94σ-121σ123σ124σ	102π108π111π-112π113π115π	106π107π111π-112π113π115π	102π108π111π-112π113π115π
5b	6 (115)	81σ85σ98σ-125σ127σ128σ	110π112π115π-117π120π121π	110π111π115π-116π117π119π	106π112π115π-116π117π119π
5c	7 (111)	80σ83σ96σ-121σ123σ124σ	108π110π111π-112π113π114π	108π110π111π-112π113π114π	105π108π111π-114π116π117π
5d	8 (115)	83σ86σ98σ-126128129	113π114π115π-116π117π118π	112π114π115π-116π117π118π	112π114π115π-118π120π121π
5e	9 (123)	89σ92σ108σ-133σ135σ136σ	120π121π122π-124π125π126π	120π121π122π-124π125π126π	120π121π122π-124π125π126π
5f	10 (115)	84σ85σ98σ-125σ127σ128σ	111π112π115π-116π117π119π	111π112π115π-116π117π120π	106π111π115π-116π117π119π
5h	11 (107)	76σ79σ92σ-117σ119σ120σ	104π106π107π-108π109π111π	104π106π107π-108π109π111π	105π106π107π-108π109π111π
5i	12 (111)	80σ81σ94σ-121σ123σ124σ	108π110π111π-112π113π115π	107π110π111π-112π113π116π	102π107π111π-116π119π125π
5j	13 (123)	88σ89σ104σ-133σ135σ136σ	114π120π123π-124π125π127π	118π119π123π-124π125π127π	114π120π123π-124π125π127π
5k	14 (119)	82σ86σ101σ-129σ131σ132σ	110π116π119π-120π121π123π	114π115π119π-120π121π123π	115π116π119π-124π125π127π
5l	15 (111)	80σ83σ96σ-121σ123σ124σ	109π110π111π-112π113π115π	109π110π111π-112π113π116π	107π108π110π-116π117π118π
5m	16 (115)	82σ86σ98σ-128σ129σ130σ	112π113π114π-116π117π118π	111π113π114π-116π117π118π	112π113π114π-116π117π118π
6a	17 (119)	83σ84σ98σ-130σ132σ133σ	115π116π119π-120π121π12	115π116π119π-120π121π124	110π116π119π-120π121π12

			3π	π	3π
6b	18 (123)	87σ88σ102σ-134σ136σ137σ	118π120π123π-125π128π129π	118π119π123π-124π125π128π	119π120π123π-127π128π132π
6c	19 (119)	85σ86σ99σ-130σ132σ133σ	116π118π119π-120π121π123π	112π113π119π-120π121π123π	116π118π119π-120π121π123π
6d	20 (123)	88σ89σ102σ-135σ137σ138σ	120π122π123π-124π125π127π	117π122π123π-124π125π127π	120π122π123π-124π125π127π
6e	21 (131)	94σ96σ111σ-142144145	121π128π130π-132π133π134π	125π128π130π-132π133π134π	128π129π130π-132π133π134π
6f	22 (123)	87σ89σ101σ-134σ136σ137σ	119π120π123π-124π125π127π	119π120π123π-124π125π128π	114π119π123π-124π125π127π

On the other hand, $(LUMO+1)^*_{30}$ is a π MO (Table 14, sixth column). A low value for $F_{30}(LUMO+1)*$ could be an indication of an unfavorable interaction of atom 30 with vacant MOs of a moiety. Then it is suggested that atom 30 is interacting in a favorable way with an electron-rich center (a π system, an anion or an electron-donor atom) through its $(LUMO)^*_{30}$. If this is the case, then η_{30} should be diminished by shifting downwards the $(LUMO)^*_{30}$ energy and keeping the condition $(HOMO)^*_{30} = HOMO$. In the case of atom 26, Table 14 shows that the occupied and vacant local MOs are very far from the frontier MOs. $(HOMO-2)^*_{26}$ is a σ MO (Table 14, third column). A small value for $S^E_{26}(HOMO-2)*$ can be interpreted by suggesting that $(HOMO-1)^*_{26}$ and $(HOMO)^*_{26}$ are engaged in attractive interactions with vacant σ MOs of the site. $(HOMO-2)^*_{26}$ seems to weaken this interaction probably through a repulsive interaction with a σ occupied MO in the site. As this atom has a noticeable positive net charge, it is expected that it interacts with a negatively charged moieties such as anions, electron-donor atoms or a π system having vacant σ MOs. An available $(LUMO+1)^*_3$ (a π MO) is taken as an indication that atom 3 is engaged in a favorable interaction with an electron-rich center through its two lowest vacant MOs. $(HOMO-1)^*_7$ is a σ or π MO. A low value for $F_7(HOMO-1)*$ is interpreted by stating that atom 7 interacts in a favorable way with an electron-deficient center through its $(HOMO)^*_7$, and that $(HOMO-1)^*_7$ weakens this interaction.

No finer interpretation is possible for the moment. All the above suggestions are displayed in the 2D partial pharmacophore shown in Fig. 16.

ISSN: 0975-8585

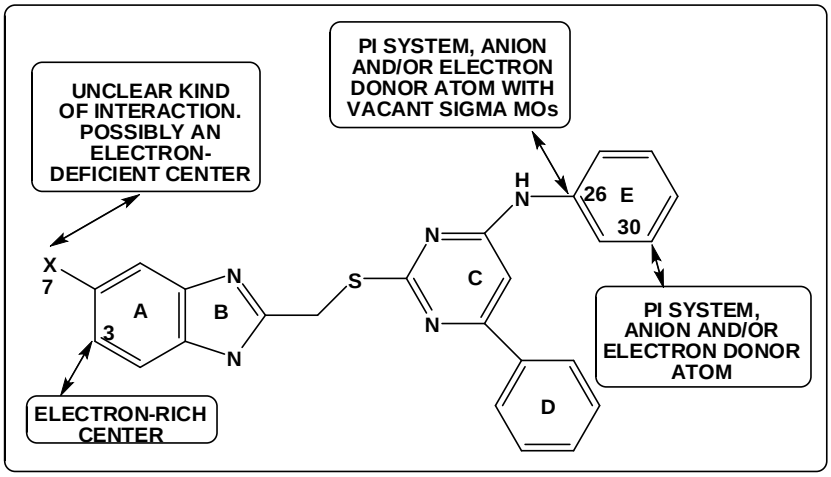

Figure 16. Partial 2D pharmacophore for the variation of the inhibitory activity against SMMC-7721 cells (Eq. 6).

MGC-803 cell line:

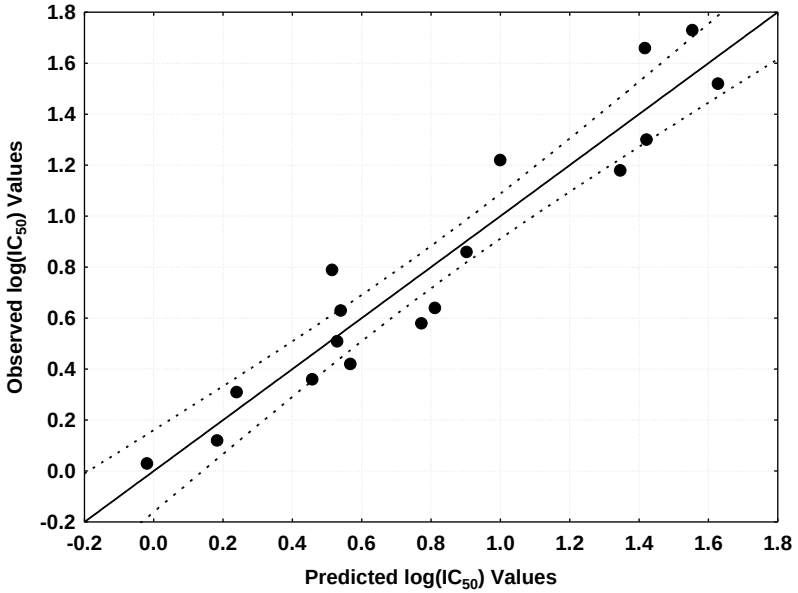

Figure 17. Observed *versus* calculated values (Eq. 7) of log (IC_{50}). Dashed lines denote the 95% confidence interval.

The best equation is:

$$\log(IC_{50}) = -7.37 + 1.33\eta_{30} - 2.10S_{12}^{E}(HOMO-1)^{*} - 0.29S_{27}^{E}(HOMO-2)^{*} - 1.06S_{17}^{E}(HOMO-2)^{*} \quad (7)$$

with n=17, R= 0.96, R^2= 0.91, adj. R^2= 0.89, F(4,12)=31.97 (p<0.000001) and a standard error of estimate of 0.18. No outliers were detected and no residuals fall outside the ±2σ limits. No significant correlation exists among independent variables. Here, η_{30} is the local hardness of atom 30, $S_{12}^{E}(HOMO-1)^{*}$ is the electrophilic superdelocalizability of the second highest occupied MO localized on atom 12, $S_{27}^{E}(HOMO-2)^{*}$ is the electrophilic superdelocalizability of the third highest occupied MO localized on atom 27 and $S_{17}^{E}(HOMO-2)^{*}$ is the electrophilic superdelocalizability of the third highest occupied MO localized on atom 17. This equation is statistically significant and the variation of the numerical

value of a group of four local atomic reactivity indices of atoms of the common skeleton explains about 89% of the variation of the inhibitory activity. Fig. 17 displays the plot of observed *vs.* calculated log(IC_{50}) values. We can see that now almost all points lie inside or close to the confidence interval. There are three exceptions.

Beta values (not shown) indicate that the importance of variables is η_{30} >> $S_{27}^{E}(HOMO-2)^{*}$ > $S_{12}^{E}(HOMO-1)^{*}$ > $S_{17}^{E}(HOMO-2)^{*}$. A high inhibitory activity is associated with low values for all four reactivity indices. A low value for η_{30} can be interpreted in the same way that in the anterior case. But, as here we have not another LARI related to atom 30, we cannot make an educated guess about the nature of the possible interaction(s). $(HOMO-2)_{27}^{*}$ is a π MO (Table 14, fourth column). A low value for $S_{27}^{E}(HOMO-2)^{*}$ suggests that atom 27 is interacting with an electron-deficient site through its first two highest occupied MOs and that an unfavorable interaction of $(HOMO-2)_{27}^{*}$ with occupied MOs of the site weakens the interaction.

$(HOMO-1)_{12}^{*}$ is a π or lone pair MO of the sulphur atom (Fig. 2 and Table 12, third column). A low value for $S_{12}^{E}(HOMO-1)^{*}$ could be an indication of an unfavorable interaction of $(HOMO-1)_{12}^{*}$ with one or more occupied MOs. Atom 12 interacts with an electron-deficient site through its $(HOMO)_{12}^{*}$. $(HOMO-2)_{17}^{*}$ is a σ MO. A low value for $S_{17}^{E}(HOMO-2)^{*}$ suggests that $(HOMO-2)_{17}^{*}$ has an unfavorable interaction with occupied MOs of the site. $(HOMO-1)_{17}^{*}$ is of σ nature and $(HOMO)_{17}^{*}$ of π nature. Atom 17 seems then to interact with an electron-deficient center. Due to the diverse nature of $(HOMO)_{17}^{*}$ and $(HOMO-1)_{17}^{*}$, the nature of the interaction cannot be established with certainty. All these suggestions are presented in the 2D partial pharmacophore shown in Fig. 18.

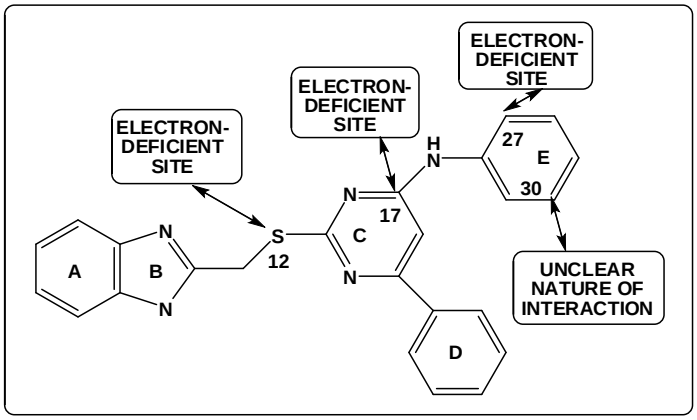

Figure 18. Partial 2D pharmacophore for the variation of the inhibitory activity against MGC-803 cells (Eq. 7).

MCF-7 cell line:

The best equation is:

$$\log(IC_{50}) = 0.97 + 0.004S_{30}^{N}(LUMO+2)^{*} + 0.69S_{7}^{E}(HOMO)^{*} + 6.92F_{4}(LUMO+2)^{*} + 0.002S_{24}^{N}(LUMO+2)^{*} - 0.39F_{28}(LUMO+1)^{*} \quad (8)$$

with n=16, R= 0.97, R^2= 0.95, adj. R^2= 0.92, F(5,10)=35.73 (p<0.000001) and a standard error of estimate of 0.12. No outliers were detected and no residuals fall outside the ±2σ limits. No significant correlation exists among independent variables. Here, $S_{30}^{N}(LUMO+2)^{*}$ is the nucleophilic superdelocalizability of the third lowest MO localized on atom 30, $S_{7}^{E}(HOMO)^{*}$ is the electrophilic superdelocalizability of the highest occupied MO localized on atom 7, $F_{4}(LUMO+2)^{*}$ is the Fukui index of the third lowest vacant MO

localized on atom 4, $S_{24}^{N}(LUMO+2)*$ is the nucleophilic superdelocalizability of the third lowest MO localized on atom 24 and $F_{28}(LUMO+1)*$ is the Fukui index of the second lowest MO localized on atom 28. This equation is statistically significant and the variation of the numerical value of a group of five local atomic reactivity indices of atoms of the common skeleton explains about 92% of the variation of the inhibitory activity. Figure 19 displays the plot of observed *vs.*

calculated log(IC_{50}) values. We can see that now almost all points lie inside or close to the confidence interval.

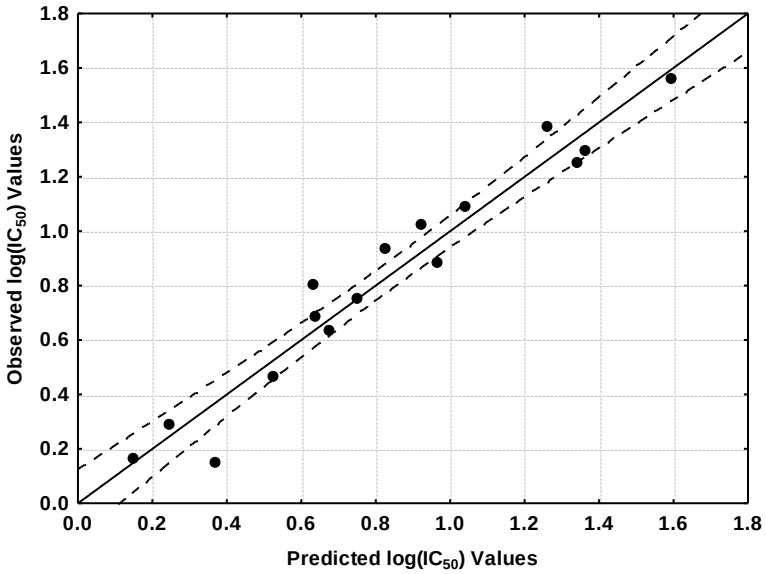

Figure 19. Observed *versus* calculated values (Eq. 8) of log (IC_{50}). Dashed lines denote the 95% confidence interval.

Beta values (not shown) indicate that the importance of variables is $S_7^E(HOMO)*$ > $F_4(LUMO+2)*$ = $S_{30}^N(LUMO+2)*$ > $S_{24}^N(LUMO+2)*$ > ($F_{28}(LUMO+1)*$). A high inhibitory activity is associated with high values for $F_{28}(LUMO+1)*$ and $S_7^E(HOMO)*$; with a low value for $F_4(LUMO+2)*$ and with reactive $(LUMO+2)_{30}^*$ and $(LUMO+2)_{24}^*$ MOs.

$F_{28}(LUMO+1)*$ will not be discussed due to its high p value (not shown). $(HOMO)_7^*$ is a σ or π MO (Table 10, sixth column). A high value for $S_7^E(HOMO)*$ suggests that in some molecules atom 7 is interacting with an electron-deficient center through its occupied frontier π local MO (a π system, a cation and/or an electron acceptor atom). If $(HOMO)_7^*$ is a σ MO and there is an interaction, it could be with a cation or with σ empty MOs. $(LUMO+2)_4^*$ is a π MO (Table 10, fourth column). A low value for $F_4(LUMO+2)*$ is suggestive of, for example, an unfavorable interaction with vacant π MOs of the site. Atom 4 interacts with an electron-rich center (a π system, an anion and/or an electron-donor atom) through its first two lowest vacant MOs. $(LUMO+2)_{30}^*$ is a π MO (Table 14, sixth column). It is suggested that atom 30 interacts with an electron-rich center (another π system, an anion and/or an electron-donor atom) through its three lowest vacant MOs.

$(LUMO+2)_{24}^*$ is a π MO (Table 13, fifth column). Atom 24 has the same kind of interactions than atom 30. Figure 20 displays the associated 2D pharmacophore.

ISSN: 0975-8585

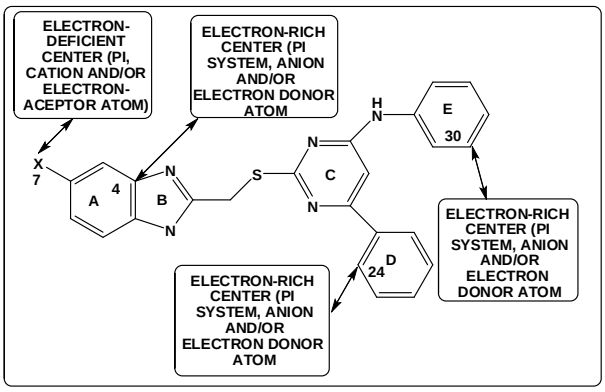

Figure 20. Partial 2D pharmacophore for the variation of the inhibitory activity against MCF-7 cells (Eq. 8).

EC-9706 cell line:

The best equation is:

$$\log(IC_{50}) = 0.92 + 0.47S_2^E(HOMO)^* + 0.005S_{30}^N(LUMO+2)^* + 4.93F_4(LUMO+2)^* + 0.71F_{23}(LUMO+2)^* \quad (9)$$

with n=16, R= 0.94, R^2= 0.89, adj. R^2= 0.85, F(4,11)=14.55 (p<0.00003) and a standard error of estimate of 0.15. No outliers were detected and no residuals fall outside the ±2σ limits. No significant correlation exists among independent variables. Here, $S_2^E(HOMO)^*$ is the electrophilic superdelocalizability of the highest MO localized on atom 2, $S_{30}^N(LUMO+2)^*$ is the nucleophilic superdelocalizability of the third lowest vacant MO localized on atom 30, $F_4(LUMO+2)^*$ is the Fukui index of the third lowest vacant MO localized on atom 4 and $F_{23}(LUMO+2)^*$ is the Fukui index of the third lowest vacant MO localized on atom 23. This equation is statistically significant and the variation of the numerical value of a group of five local atomic reactivity indices of atoms of the common skeleton explains about 85% of the variation of the inhibitory activity. Fig. 21 displays the plot of observed *vs.* calculated log(IC_{50}) values. We can see that now almost all points lie inside or close to the confidence interval. There is a point located relatively far from the confidence interval.

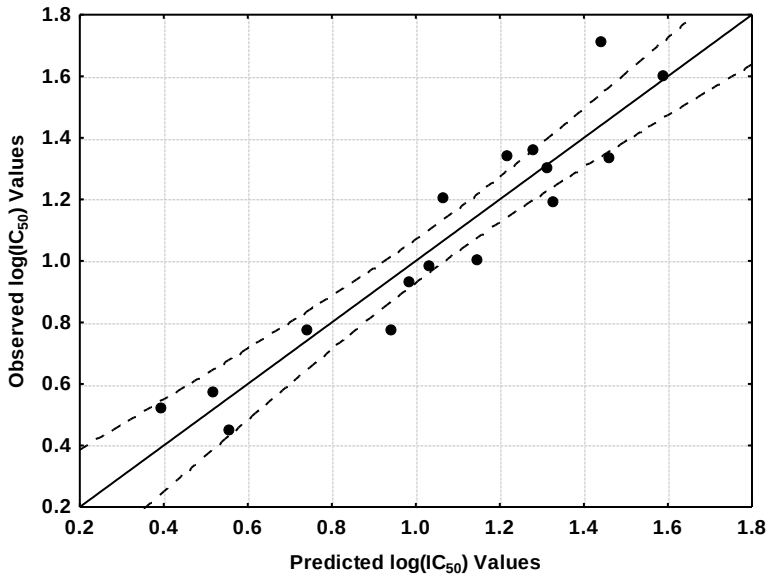

Figure 21. Observed *versus* calculated values (Eq. 9) of log (IC_{50}). Dashed lines denote the 95% confidence interval.

ISSN: 0975-8585

Beta values (not shown) indicate that the importance of variables is $S_2^E(HOMO)*$ > $S_{30}^N(LUMO+2)*$ > $F_4(LUMO+2)*$ > ($F_{23}(LUMO+2)*$). A high inhibitory activity is associated with a high value for $S_2^E(HOMO)*$, low values for $F_4(LUMO+2)*$ and $F_{23}(LUMO+2)*$ and with an available $(LUMO+2)_{30}^*$ MO for interactions. $F_{23}(LUMO+2)*$ will not be discussed due to its high p value (not shown). $(HOMO)_2^*$ is a π MO (Table 10, third column). A high value for $S_2^E(HOMO)*$ suggests that atom 2 interacts with an electron-deficient moiety (another π system, an anion and/or an electron donor atom for example). $(LUMO+2)_{30}^*$ is a π MO (Table 14, sixth column). The analysis is the same than for the anterior cell line case: atom 30 interacts with an electron-rich center (a π system, an anion and/or an electron-donor atom) through its three lowest vacant MOs. $(LUMO+2)_4^*$ is a π MO (Table 10, fourth column). A low value for $F_4(LUMO+2)*$ suggests an unfavorable interaction of $(LUMO+2)_4^*$ with vacant MOs of the site. Atom 4 in interacting in a favorable way with an electron-rich center through its two lowest vacant MOs. Figure 22 displays the corresponding 2D pharmacophore.

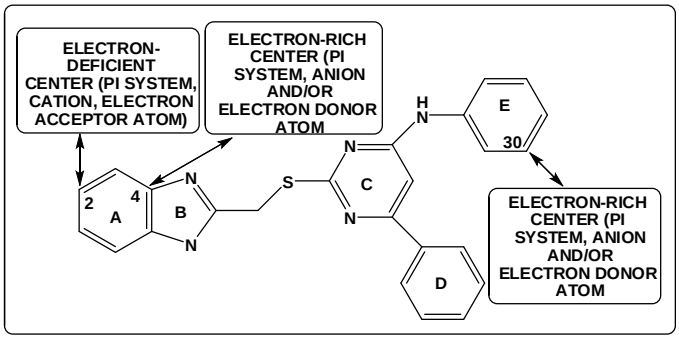

Figure 22. Partial 2D pharmacophore for the variation of the inhibitory activity against SEC-9706 cells (Eq. 9).

The enlarged skeleton has risen the percentage of explanation in three of four cases. In SMMC-7721 cells the percentage of explanation rose from 82% to 95%, in MGC-803 cell from 70% to 89% and in MCF-7 cell from 78% to 92%. In the case of SEC-9706 cells, the percentage diminished from 90% to 85%. Now, if we merge the two partial pharmacophores of each cell line, we obtain the final pharmacophores shown in Figs. 23-26.

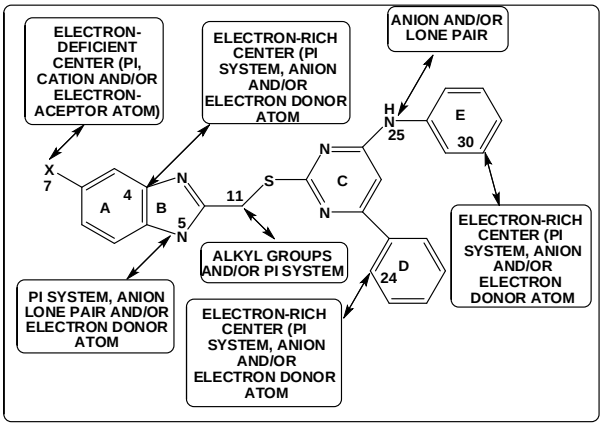

Figure 23. Partial 2D pharmacophore for the variation of the inhibitory activity against MCF-7 cells obtained by the merging the corresponding two pharmacophores.

ISSN: 0975-8585

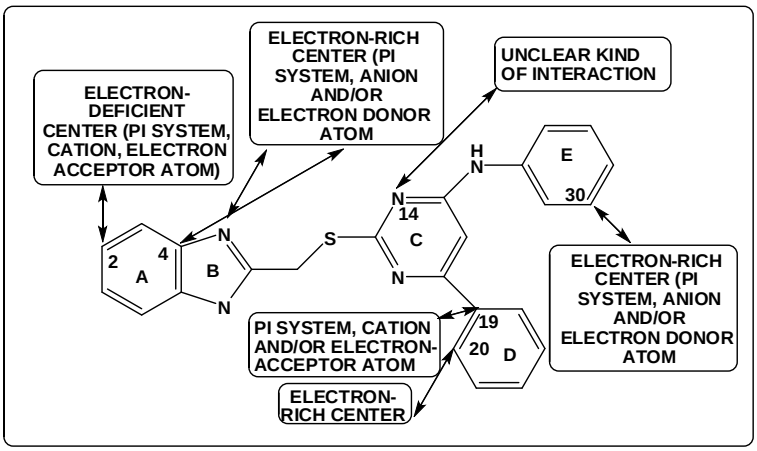

Figure 24. Partial 2D pharmacophore for the variation of the inhibitory activity against EC-9706 cells obtained by the merging the corresponding two pharmacophores.

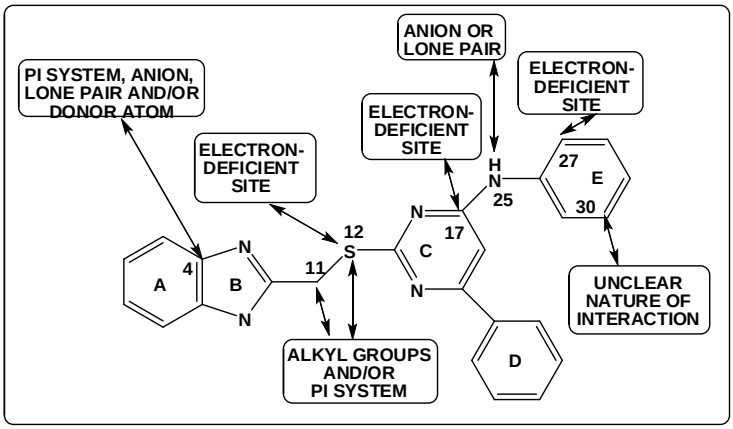

Figure 25. Partial 2D pharmacophore for the variation of the inhibitory activity against MGC-803 cells obtained by the merging the corresponding two pharmacophores.

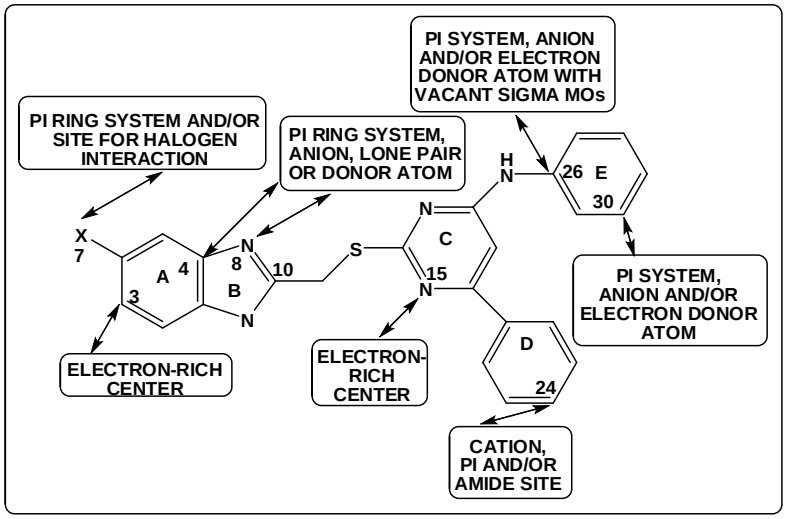

Figure 26. Partial 2D pharmacophore for the variation of the inhibitory activity against SMMC-7721 cells obtained by the merging the corresponding two pharmacophores.

It is interesting to note that for each cell line there are no contradictions among the two corresponding partial pharmacophores. Accepting that for a given cell line all molecules exert their inhibitory

activity at the same (unknown) site, it is not necessary that the common skeleton interacts with the same moieties of the site. In a very recent QSAR and docking study of *N*-benzylphenethylamines interacting with the 5-HT_{2B} receptor (unpublished) it is shown that, for example, a given atom or moiety of the common skeleton is able to have the same kind of interaction but with different amino acids. Then, for cases such as atom 7 (see Fig. 2), there can be different sites for the interaction with π or σ MOs. Also, it was shown that a given moiety of *N*-benzylphenethylamines can interact with two or more residues in different ways. In the cases studied here, the lack of knowledge of the action mechanism(s) does not allow to go deeper in our analysis. A last general comment. It is curious to notice that in most papers reporting cytoxicity and/or antiproliferative activity of series of molecules results concerning healthy cell lines are not presented. We understand that the final scope of these kinds of studies is finding compounds with action(s) against tumoral cells without harming normal ones.

CONCLUSIONS

We have obtained statistically significant results for the antiproliferative activity of the title compounds against four human cancer cell lines. From the results the corresponding 2D partial pharmacophores associated with high inhibitory activity have been built. These structures should help the experimentalists in the search of new compounds. The nature of the results obtained here strongly suggests that the molecules act at a single site in each cell line.

REFERENCES

[1] AM Alafeefy; AE Ashour; O Prasad; L Sinha; S Pathak, et al., Eur. J. Med. Chem., 2015, 92, 191-201.
[2] KM Amin; SM Abou-Seri; FM Awadallah; AAM Eissa; GS Hassan; MM Abdulla, Eur. J. Med. Chem., 2015, 90, 221-231.
[3] D Bandyopadhyay; JL Sanchez; AM Guerrero; F-M Chang; JC Granados, et al., Eur. J. Med. Chem., 2015, 89, 851-862.
[4] R Bollu; JD Palem; R Bantu; V Guguloth; L Nagarapu, et al., Eur. J. Med. Chem., 2015, 89, 138-146.
[5] H Chen; F Xu; X Liang; B-B Xu; Z-L Yang, et al., Bioorg. Med. Chem. Lett., 2015, 25, 285-287.
[6] K-G Cheng; C-H Su; L-D Yang; J Liu; Z-F Chen, Eur. J. Med. Chem., 2015, 89, 480-489.
[7] WM Eldehna; A Altoukhy; H Mahrous; HA Abdel-Aziz, Eur. J. Med. Chem., 2015, 90, 684-694.
[8] WM Eldehna; HS Ibrahim; HA Abdel-Aziz; NN Farrag; MM Youssef, Eur. J. Med. Chem., 2015, 89, 549-560.
[9] MM Gamal El-Din; MI El-Gamal; MS Abdel-Maksoud; KH Yoo; C-H Oh, Eur. J. Med. Chem., 2015, 90, 45-52.
[10] E Hejchman; P Taciak; S Kowalski; D Maciejewska; A Czajkowska, et al., Pharmacological Reports, 2015, 67, 236-244.
[11] X-C Huang; L Jin; M Wang; D Liang; Z-F Chen, et al., Eur. J. Med. Chem., 2015, 89, 370-385.
[12] MM Kandeel; HM Refaat; AE Kassab; IG Shahin; TM Abdelghany, Eur. J. Med. Chem., 2015, 90, 620-632.
[13] D Kathirvelan; J Haribabu; BSR Reddy; C Balachandran; V Duraipandiyan, Bioorg. Med. Chem. Lett., 2015, 25, 389-399.
[14] RM Kumbhare; TL Dadmal; MJ Ramaiah; KSV Kishore; SNCVL Pushpa Valli, et al., Bioorg. Med. Chem. Lett., 2015, 25, 654-658.
[15] K Kuroiwa; H Ishii; K Matsuno; A Asai; Y Suzuki, ACS Med. Chem. Lett., 2015,
[16] C Le Floch; E Le Gall; S Sengmany; P Renevret; E Léonel, et al., Eur. J. Med. Chem., 2015, 89, 654-670.
[17] AM Mahran; SS Ragab; AI Hashem; MM Ali; AA Nada, Eur. J. Med. Chem., 2015, 90, 568-576.
[18] A Martorana; C Gentile; U Perricone; AP Piccionello; R Bartolotta, et al., Eur. J. Med. Chem., 2015, 90, 537-546.
[19] VFS Pape; D Türk; P Szabó; M Wiese; EA Enyedy; G Szakács, J. Inorg.Biochem., 2015, 144, 18-30.
[20] AM Sajith; KK Abdul Khader; N Joshi; MN Reddy; M Syed Ali Padusha, et al., Eur. J. Med. Chem., 2015, 89, 21-31.
[21] Shamsuzzaman; A Mashrai; H Khanam; M Asif; A Ali, et al., J. King Saud Univ. Sci., 2015, 27, 1-6.
[22] JB Shi; WJ Tang; XB qi; R Li; XH Liu, Eur. J. Med. Chem., 2015, 90, 889-896.
[23] Y Song; Z Xin; Y Wan; J Li; B Ye; X Xue, Eur. J. Med. Chem., 2015, 90, 695-706.
[24] G-H Yan; X-F Li; B-C Ge; X-D Shi; Y-F Chen, et al., Eur. J. Med. Chem., 2015, 90, 251-257.
[25] DI Pino-Ramírez; JS Gómez-Jeria, Amer. Chem. Sci. J., 2014, 4, 554-575.

[26] D Muñoz-Gacitúa; JS Gómez-Jeria, J. Comput. Methods Drug Des., 2014, 4, 48-63.
[27] D Muñoz-Gacitúa; JS Gómez-Jeria, J. Comput. Methods Drug Des., 2014, 4, 33-47.
[28] JS Gómez-Jeria; J Valdebenito-Gamboa, Der Pharma Chem., 2014, 6, 383-406.
[29] JS Gómez-Jeria, J. Comput. Methods Drug Des., 2014, 4, 38-47.
[30] JS Gómez-Jeria, Der Pharma Chem., 2014, 6, 64-77.
[31] JS Gómez-Jeria, Brit. Microbiol. Res. J., 2014, 4, 968-987.
[32] JS Gómez-Jeria, Int. Res. J. Pure App. Chem., 2014, 4, 270-291.
[33] F Gatica-Díaz; JS Gómez-Jeria, J. Comput. Methods Drug Des., 2014, 4, 79-120.
[34] JS Gómez-Jeria; M Flores-Catalán, Canad. Chem. Trans., 2013, 1, 215-237.
[35] K-P Shao; X-Y Zhang; P-J Chen; D-Q Xue; P He, et al., Bioorg. Med. Chem. Lett., 2014, 24, 3877-3881.
[36] JS Gómez-Jeria, Canad. Chem. Trans., 2013, 1, 25-55.
[37] JS Gómez-Jeria, Elements of Molecular Electronic Pharmacology (in Spanish), Ediciones Sokar, Santiago de Chile, 2013.
[38] T Bruna-Larenas; JS Gómez-Jeria, Int. J. Med. Chem., 2012, 2012 Article ID 682495, 1-16.
[39] JS Gómez-Jeria, Int. J. Quant. Chem., 1983, 23, 1969-1972.
[40] JS Gómez-Jeria, Il Far. (Ed. Sci). 1985, 40, 299-302.
[41] JS Gómez-Jeria, "Modeling the Drug-Receptor Interaction in Quantum Pharmacology," in Molecules in Physics, Chemistry, and Biology, J. Maruani Ed., vol. 4, pp. 215-231, Springer Netherlands, 1989.
[42] JS Gómez-Jeria; M Ojeda-Vergara; C Donoso-Espinoza, Mol. Engn., 1995, 5, 391-401.
[43] JS Gómez-Jeria; M Ojeda-Vergara, J. Chil. Chem. Soc., 2003, 48, 119-124.
[44] MJ Frisch; GW Trucks; HB Schlegel; GE Scuseria; MA Robb, et al., Gaussian98 Rev. A.11.3, Gaussian, Pittsburgh, PA, USA, 2002.
[45] JS Gómez-Jeria, D-Cent-QSAR: A program to generate Local Atomic Reactivity Indices from Gaussian log files. 1.0, Santiago, Chile, 2014.
[46] JS Gómez-Jeria, J. Chil. Chem. Soc., 2009, 54, 482-485.
[47] Statsoft, Statistica 8.0, 2300 East 14 th St. Tulsa, OK 74104, USA, 1984-2007.
[48] U Varetto, Molekel 5.4.0.8, Swiss National Supercomputing Centre: Lugano, Switzerland, 2008.
[49] RD Dennington; TA Keith; JM Millam, GaussView 5.0.8, GaussView 5.0.8, 340 Quinnipiac St., Bldg. 40, Wallingford, CT 06492, USA, 2000-2008.
[50] Hypercube, Hyperchem 7.01, 419 Phillip St., Waterloo, Ontario, Canada, 2002.
[51] Chemaxon, MarvinView, www.chemaxon.com, USA, 2014.
[52] E Joselevich, ChemPhysChem, 2004, 5, 619-624.
[53] E Joselevich, Ang. Chem. Int. Ed., 2004, 43, 2992-2994.